Membrane Transfer Process for the Creation of Low-Noise Solid State Nanopore Devices

by

Tarun Jain

B.A. Mathematics, Physics New York University, 2009

Submitted to the Department of Mechanical Engineering
in partial fulfillment of the requirements for the degree of

Master of Science in Mechanical Engineering

at the

MASSACHUSETTS INSTITUTE OF TECHNOLOGY

May 2011
[June 2011]

Author .....
Department of Mechanical Engineering
May 31, 2011

Certified by .....
Professor Rohit Karnik
d'Arbeloff Assistant Professor of Mechanical Engineering
Thesis Supervisor

Accepted by .....
Professor David E. Hardt
Graduate Officer, Department of Mechanical Engineering

Abstract

Membrane Transfer Process for the Creation of Low-Noise Solid State Nanopore Devices

Tarun Jain

Nanopore sensors are an emerging technology whereby the modulation of a current trace upon passage of the analyte through the nanopore is used to infer the properties of the analyte. This technology is particularly attractive because it is label-free, rapid, and intrinsically single molecule. However, the ability to infer molecular properties with nanometer precision, either in size or sequencing, is obscured by noise in the measurement. The precision of this inference can be significantly improved by reducing noise and by performing multiple measurements on the same molecule. Solid state nanopores, made in free standing membranes, however, have traditionally exhibited high levels of capacitive noise at 100 kHz bandwidths, as well as poor confinement of the electric field around the nanopore. In this thesis, a novel device concept is designed for creating solid state nanopores whereby the free standing membrane is transferred over a PDMS microchannel. By eliminating the silicon wafer backing, capacitive noise is dramatically reduced. Furthermore, the microchannel confines the electric field outside the nanopore, thereby enhancing the ability to perform multiple measurements.

Acknowledgments

I would like to express my sincere gratitude to those people who have made this thesis possible. My research advisor, Prof. Rohit Karnik has acted as the epitome of the modern researcher. While granting the license of free thought and scientific inquiry, he also watches carefully, ready to lend a guiding hand. His trust and friendship have inspired me. I am also grateful to Dr. Carlos Aguilar for his efforts on the project. I would also like to thank all my lab mates, and in particular Suman, Marco, Sean, and Jongho. Finally, I would like to acknowledge my family, for it is their care and thoughtfulness that has defined my being.

Contents

List of Figures

Chapter 1

Introduction

1.1 Background

Consisting of a nanometer sized aperture in a thin dielectric membrane immersed in electrolyte solution, nanopore sensors are an emerging tool for measuring the structural properties of individual biomolecules. An applied electric field transverse to the nanopore establishes a current of ions which is simultaneously recorded using a low noise, high gain amplifier. Upon passage through the nanopore (translocation), analyte molecules in solution modulate the measured ionic current. Structural properties of the molecule are then inferred from the modulated ionic current signal.

Nanopore sensors are a particularly attractive tool for molecular analysis due to their ability to perform direct electrical measurements on single molecules. Unlike many modern analysis methods, the analyte sample does not need to be fluorescently labeled or amplified using PCR. Nanopore sensors are intrinsically single molecule, which means that it is possible to measure variations of molecular properties within a specific type of molecule can be detected. The potential for high-throughput DNA sequencing on large fragments has been one of the dominant driving factors in nanopore

research. The other dominant application is the ability to measure the length or size of biomolecules. In both cases, the highest aim is to achieve sub-nanometer spatial resolution on the molecule of interest.

In 1996, Kasianowicz performed the first characterization of DNA molecules in nanopore sensors using α-hemolysin, a 1.5 nm diameter ion channel naturally occurring *Staphylococcus aureus* bacteria[1]. Using a genetically engineered and adapted variant of α-hemolysin, Clarke et. al. demonstrated the ability to use nanopore sensors for single nucleotide discrimination[2]. Derrington et. al. demonstrated a similar ability to discriminate nucleotides in another biological ion channel, MspA[3]. Owing to the self-assembly process which governs their formation, biological ion channels of the same type are chemically and structurally identical, enabling a high degree of repeatability.

However, biological ion channels are extremely sensitive to changes in ionic concentration, pH, transmembrane potential, mechanical stresses, and temperature, and thereby prone to failure[4]. Furthermore, the range of possible analytes is restricted by the diameter of the biological ion channel, which is rarely larger than a couple of nanometers. These limitations have driven interest in the fabrication of nanopores in inorganic dielectric membranes, often referred to as solid state nanopores.

Collimated ion and electron beams have allowed for control and visualization of solid state nanopores with precision down to the sub-5 nanometer regime. Solid state nanopores have displayed superior stability and life-times compared to their biological counterparts. The main challenge for nanopore sensors lies in the ability to accurately assign molecular properties of molecules based on the recorded ionic current, particularly in the presence of large levels of capacitive and flicker noise. Nanopore sensors fundamentally rely on the statistical relationship between the current modulation and analyte structure. Theory states that the instantaneous current is related to the average cross sectional area of the analyte species within the nanopore. Thus the primary ap-

plications of nanopore sensors are the measurement of the instantaneous average cross sectional area of the analyte as a function of the analyte length, or to measure the total volume of the analyte. In the context of DNA, these applications refer to DNA sequencing and DNA sizing respectively. The ability to perform DNA sequencing and sizing with direct, label-free measurements at the single molecule level has the ability to dramatically reduce costs, increase throughput, and allow for device portability. The use of these nanopore sensors, however, can be extended to nearly any kind of analyte molecule.

The accuracy of measurements in nanopores (and hence the resolution with which size and sequencing measurements can be made) is significantly limited by poor signal to noise ratios. The electrophoretic velocity of the analyte molecule determines both the mean translocation duration and the length of the molecule that travels through the nanopore at a given bandwidth. Higher bandwidths therefore directly imply higher spatial resolution. Higher measurement bandwidths, however, also lead to larger noise levels, thereby degrading the overall signal to noise ratio.

Improving the signal to noise ratio will allow for the detection of smaller molecules with larger nanopores at 100 kHz, thereby increasing spatial resolution with a greater dynamic rage of the nanopore sensor. In general, there are three approaches through which the poor signal quality can be improved:

1. Improve Signal Quality

2. Decrease Noise Levels

3. Measure the Same Molecule Multiple Times

Till date, research has been focused on improving the statistical inference by increasing the relative magnitude of the translocation signal. A recent example is a membrane which was locally thinned to obtain nanopore dimensions of 8 nm thickness and 4 nm

diameter[5]. Improved signal size typically means obtaining thinner nanopores with a large area of the nanopore being blocked by the analyte molecule upon translocation. Similarly, several groups have been working on graphene nanopores[6, 7, 8]; being atomically thin, graphene nanopores represent the limits of molecular spatial resolution. However, at high bandwidths (> 10 kHz) capacitive noise from the silicon wafer handle becomes the dominant source of noise in these systems[9, 10, 11]. Furthermore, the ability to perform multiple measurements on the same molecule is inhibited by the poor confinement of the electric field outside the nanopore in membrane based devices [12]. It is important to note that the capacitive noise from the silicon wafer, and the poor confinement of the electric field, are intrinsic to the basic structure of a membrane based nanopore device, i.e. the wide open area of the membrane exposed to the ionic solution. While further nanofabrication may in principle be used to partially improve the results, in practice this adds significantly to the cost of the devices and decreases device throughput.

Therefore the goal of this work is to design a new type of nanopore device which addresses the shortcomings of traditional membrane based pores in an effective manner. In particular, the new type of device should reduce the capacitive noise from the silicon wafer, and confine the electric field around the nanopore for higher recapture probabilities. And finally, the device fabrication should be amenable to being scaled up to wafer level fabrication as well as being cost-effective.

1.2 Device Concept

In this thesis, a novel type of nanopore sensor is designed, whereby the transfer of solid state membranes with nanopores into microfluidic devices is demonstrated to

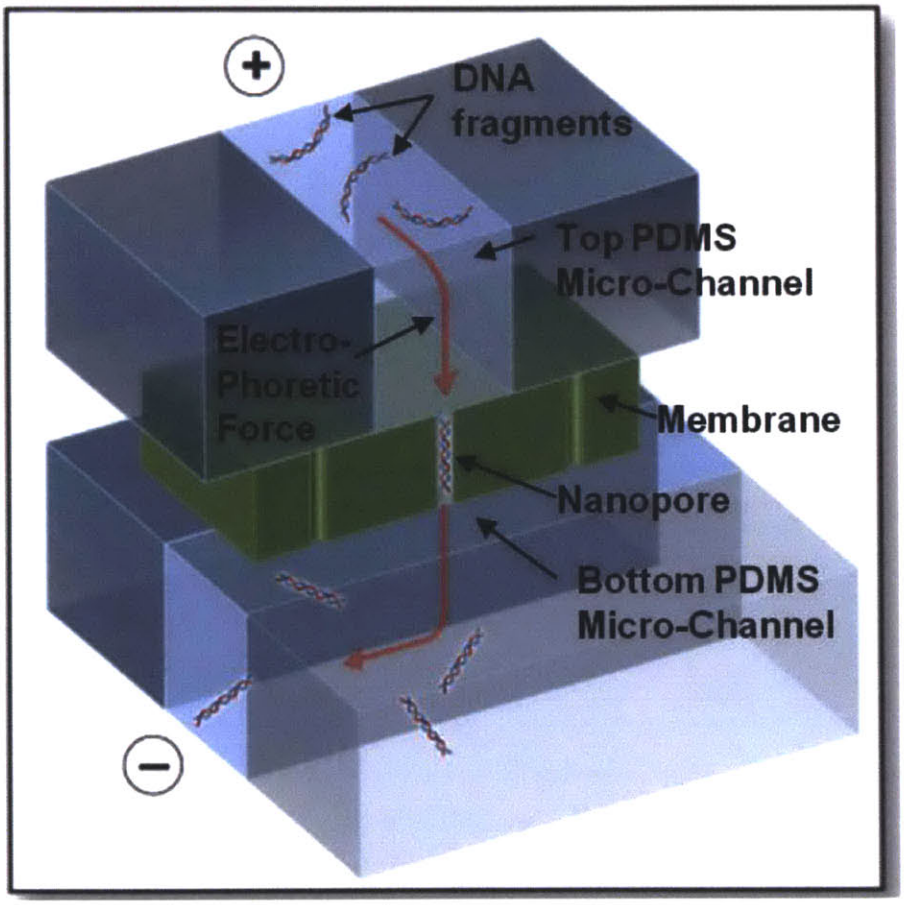

Figure 1.1: Schematic illustrating device concept. Artwork by Chester Beals, MIT LL

significantly decrease high-bandwidth noise and improve the ability to perform multiple measurements on the same molecule. Figure 1.1 illustrates a single nanopore isolated between the intersection of two perpendicular microchannels, allowing for a well defined geometric environment surrounding the nanopore.

First, the theory for statistical inference of molecular properties will be presented, and from it, a conceptual picture of noise in nanopore devices will emerge. A generalized noise model for nanopore devices is constructed and used to hypothesize noise levels resulting from the membrane transfer process. In particular, transferring the membrane between two perpendicular microchannels removes the silicon wafer handle and restricts the area exposed to fluid. This results in an increase in the resistance of the constant phase element in parallel to the nanopore, thereby virtually eliminating capacitive noise. The theory for performing multiple measurements will further illustrate how the microchannels around the transferred nanopore confine the electric field, resulting in an improved ability to perform multiple measurements on the same molecule.

Following the motivation for the work, a specific fabrication method for realizing this device concept will be presented. This will begin with the fabrication of the nanopores using the focused ion beam. Creating a predefined square array of nanopores is a critical part in attaining large alignment tolerances (50 μm) in the fabrication process. Atomic Layer Deposition was then used to tune the surface properties and shrink the nanopore. The evolution from design considerations to fabrication techniques and the membrane transfer process will be presented. The design considerations specifically relate to the ease of fabrication and ability to extend the current work to wafer scale fabrication of nanopore devices in parallel. At its core, the benefits of this work arise from the transfer of the membrane into a geometrically controlled environment. The fabrication procedure presented will demonstrate a reduction of this idea into practice.

Finally, the noise levels in the membrane transfer devices are tested and compared with hypothesized equilibrium noise levels. Measurements of DNA translocation in the device demonstrate the readiness of the platform for extended studies on analyte properties.

In accordance with the aims, the general device concept is to essentially detach the membrane from its silicon wafer backing and deposit it over a microchannel in a polymeric substrate (in this case, polydimethylsiloxane, PDMS). A second PDMS piece with a microchannel perpendicular to the first can then be places over the membrane, thereby encapsulating a single nanopore between two microfluidic channels. Should this conceptual design be achievable, we would anticipate that the capacitive noise from the silicon wafer would be eliminated, since now it simply isn't there. Furthermore, PDMS has a low dissipation factor of 0.002, which is on the order of quartz and glass. Therefore, we further anticipate that the capacitive noise from the PDMS substrate will be minimal. The device design has the further advantage that the microchannels define the electric field outside of the nanopore. The microchannel width and height can be altered to obtain the desired electric field strength outside the nanopore, and the length of the microchannel can be tuned to pick the desired voltage drop through the microchannel compared to through the nanopore. This design has the additional benefit of allowing for seamless integration of the nanopore with microfluidics: enabling both integrated sample preparation and active transport of analytes to the nanopore.

Chapter 2

Signal and Noise Theory

The fundamental premise of nanopore sensors is that the structural properties of an analyte molecule can be inferred from its translocation signal. Here, the relationship between local molecular properties and the measured ionic current will be explicitly derived under a mean field description.

2.1 Current Modulation in Nanopores

The electrolyte solution which the nanopore is immersed in contains a variety of molecular species, divided principally into ions and analytes. Upon application of an electric field, the current through the nanopore can be written using classical statistical mechanics as a sum over all ions in solution:

$$I = e \int \left(\sum_j n_j z_j v_j \right) dA_j \tag{2.1}$$

The meaning of each symbol, and in particular, the form of the concentration, n_j, is given in Table 2.1. To calculate the total current at any instance in time using the expression above would require that the complete distribution of ion positions and their

Variable	Symbol
I	Current through nanopore
e	Charge of an electron
i^C	Counter ion species
$n_j = \delta(\vec{x} - \vec{x}_j)$	Number density of the i^{th} species (within the nanopore)
$p_j(\vec{x})$	Ensemble averaged probability of finding the j^{th} ion in position $\vec{x}$
N_i	Number of ions of the i^{th} species
$n_i(\vec{x}) = N_i p_j$	Ensemble averaged concentration of the i^{th} species
$\bar{n}_i$	Mean (cross sectionally averaged) concentration of the i^{th} species
z_i	Valency of the i^{th} species
z_a	Valency of the analyte molecule
λ_a	Linear charge density of analyte species
A_i	Area of available for occupancy to the i^{th} species
A_a	Mean cross-sectional area of analyte in nanopore
v_j	Velocity of the j^{th} ion in the nanopore
$\bar{v}_i = \mu_i E$	Mean drift velocity of an ionic species
μ_i	Electrophoretic mobility of the i^{th} species
E	Electric field transverse to the nanopore
ϕ	Fraction of Mobile Counter Ions around Analyte
l	Length of Analyte Molecule
L	Length of nanopore

Table 2.1: Variables for Current Modulation Theory

velocities be known. Since obtaining knowledge of the partition function or the particle distributions is a non-trivial endeavor, it is preferable to obtain approximations which appropriately reflect the relevant physical scaling. Thus, the delta function form of the number density is first converted to a position dependent ensemble averaged position dependent probability:

$$I = e \int \left(\sum_j p_j z_j v_j \right) dA_j \tag{2.2}$$

Since exchange of ions of the same species doesn't change the current ($p_j = p_i$), the current can be re-written as the sum over all species by introducing the ensemble averaged number density:

$$I = e \int \left(\sum_i n_i z_i \bar{v}_i \right) dA_i \tag{2.3}$$

Finally, the position dependent number density, n_i is approximated as the cross-sectionally averaged number density, $\bar{n}_i$ in order to perform the integration and obtain a simplified expression for the current:

$$I = e \sum_i \bar{n}_i z_i \bar{v}_i A_i \tag{2.4}$$

$$I = eE \sum_i \bar{n}_i z_i \mu_i A_i \tag{2.5}$$

Re-writing this expression will yield Ohm's law and the expression for the conductivity. While equation 2.5 might seem like an oversimplification, much of the complexity has been well hidden within the use of these mean field parameters, such as the number density and the electrophoretic mobility.

The utility of the analytic form therefore comes from its ability to provide order of

magnitude estimates by using free solution estimates for the electrophoretic mobility, and simple charge conservation to estimate the effects of pore surface charge on the number density inside the nanopore. Furthermore, the analytic model provides scaling and insight into the effects of nanopore geometry. As will be seen later, the expression will also provide some insight into the origins of noise. It is primarily when the finite size of the ion can no longer be neglected, and the continuum approximation break down that one needs to revert back to a full statistical mechanical treatment to obtain estimates of the current.

Note that the electric field transverse to the nanopore is roughly uniform through the length of the nanopore assuming that the concentration of ions is uniform across the length of the nanopore. Furthermore, the cross sectional area A_i is defined as being dependent on the species. This was notationally included to emphasize that the cross-sectional area occupied by the ions and the analyte differs. Now let us include the contribution of the analyte molecule alongside the sum over all ionic species. Thus, let the sum over i be over all ions in the electrolyte solution, and let variables with the subscript a represent those values belonging to the analyte molecule:

$$I = eE\left[\sum_i \bar{n}_i(a)\, z_i \mu_i (A - A_a) + \lambda_a \mu_a A_a\right] \tag{2.6}$$

The functional dependence, $\bar{n}_i(a)$ refers to the fact that the translocation of an analyte molecule changes the mean concentration of ions in the nanopore. During translocation, however, the analyte molecule also excludes the ions in the nanopore from its own volume. This exclusion is analytically expressed by the subtraction of the cross sectional area of the analyte, A_a, from the cross-sectional area of the nanopore. Since the concentration of ions has already been averaged over the cross section of the nanopore, the expression above cannot adequately represent the variation in current modulation caused by the position within the cross section which the analyte occupies

in the nanopore. However, this assumption should not affect the mean translocation amplitude, and if continuum current varies significantly as a function of the relative position of the DNA to the nanopore walls, then its effects can likely be represented by an additional source of noise.

The last piece of this analytic expression is to determine what the function $\bar{n}_i(a)$ is. In the case of DNA, the Manning-Oosawa Condensation Factor[13] describes the fraction of counter-ions surrounding the DNA molecule which are mobile. Let this fraction of mobile counter ions be ϕ, and the total number of such counter ions be $\frac{\lambda_a}{z_{iC}}\phi$. These counter-ions are then assumed to be distributed equally along the analyte molecule's length, in which case the analyte contributes $\frac{\lambda_a}{z_{iC}}\phi$ mobile counter-ions to the cross section of the nanopore. Therefore, the current becomes:

$$I = eE\left[\sum_i \left(\bar{n}_i + \frac{\lambda_a}{z_i}\phi\,\delta\left(i = i^C\right)\right) z_i\mu_i\left(A - A_a\right) + \lambda_a\mu_a A_a\right] \tag{2.7}$$

Note that this expression holds only if there is one counterion species in the solution. If this is not the case, then we would have to add the additional complication of the fractions of each counterion species which screen the analyte charge in solution to the expression. It is important to note that so far, we have assumed an infinitely thin nanopore.

2.1.1 Interpretive Remarks: Sequencing

One of the major applications of nanopore sensors has been their potential for obtaining high-throughput genomic data on a single cell level without labeling or amplification. Mathematically, DNA sequencing through a nanopore is equivalent to measuring $A_a(x)$, where x is a variable that spans the length of the molecule. In other words, sequencing with nanopores relies on the ability to measure variations in the cross sectional area

of the analyte molecule as a function of its length. In the ensemble averaged ionic current description above, the ionic current is only sensitive to the *mean occupied* cross sectional area of the analyte molecule in the nanopore.

Therefore, there are two key parameters of interest in this case. The first is the ability to discriminate variations in the mean occupied cross sectional area. Some general *a priori* knowledge of the molecular structure allows for an estimate of the size of the variation in cross sectional area δA over a length δx of the molecule. Sequencing then requires the difference in the measured currents for a given cross sectional area be greater than the peak to peak noise, I_{PP} in the ionic current measurement.

$$\Delta I = I\left(A_a + \delta A_a\right) - I\left(A_a\right) > 2\delta I_{PP} \tag{2.8}$$

Prior to the introduction of the analyte molecule, noise characterization of the nanopore device allows for an estimate of the peak to peak noise in the ionic current at any given bandwidth. In this case, the minimum measurement bandwidth is given as a function of the desired length resolution, δx of the analyte as:

$$B > \frac{\delta x}{\mu_a E} \tag{2.9}$$

At high concentrations, the contribution to the current from mobile counter-ions can be considered negligible, and the resulting performance criteria becomes:

$$\Delta I = eE\delta A_a \left(\lambda_a \mu_a + \sum_i \mu_i z_i \bar{n}_i\right) > 2\delta I_{PP} \tag{2.10}$$

With appropriate measurements of electrophoretic mobilities of the DNA and a calibrated model for the noise in nanopore systems, this criterion can be evaluated analytically to predict the extent of success. It is important to note, however, that the resolution in terms of length along the DNA molecule will typically be limited by the

length of the nanopore, as in the equation above, the value δA_a is the change in cross sectional area after averaging over the volume of the analyte molecule which is inside the nanopore. Thus, the smallest constriction of the nanopore should be atomically thin. Lastly, in this case we have assumed that the analyte molecule can only pass through the nanopore with one configuration. This is true for DNA if the pore size is sufficiently small to geometrically exclude folded DNA from translocating through the nanopore.

Interestingly, the same kind of calculation could have been performed in the low concentration limit, where instead of variations in cross sectional area across the analyte length, variations in surface charge would be measured.

2.1.2 Interpretive Remarks: Sizing

The second application of nanopore sensors is the ability to measure the size of the analyte molecule. While sequencing of polymeric analyte species is optimally done in small pores on the order of the cross section of the unfolded polymer, for sizing it may be preferable for the nanopore cross section to be as large as possible (provided the analyte species can be detected compared to the noise background). The larger the nanopore, the larger the cross-section of the analyte molecule that can be accepted by the pore. Thus, larger pore cross-sectional areas allow for greater dynamic range and platform flexibility as a sizing method. If only a specific type of analyte needs to be analyzed, then large pore dynamic range can be traded for smaller pores whose size optimizes signal magnitude.

Unlike sequencing, sizing does not impose a fundamental restriction on the length of the nanopore. In the case where the entire molecule fits inside the nanopore within the duration of the translocation, the current during translocation can be expressed as a function of the fractional length occupied by the molecule $\Phi = \frac{l}{L}$ and the mean cross

sectional area occupied by the analyte molecule, A_a:

$$I = eE\left[\sum_i \left(\bar{n}_i + \frac{\lambda_a}{z_i}\phi\,\delta\left(i = i^C\right)\right) z_i\mu_i\left(A - A_a\Phi\right) + \lambda_a\mu_a A_a\Phi\right] \tag{2.11}$$

From this current, the translocation amplitude (change in current due to translocation) can be derived as:

$$\Delta I = eE\Phi A_a\left[\sum_i \left(\bar{n}_i + \frac{\lambda_a\phi}{z_i}\delta\left(i = i^C\right)\right) z_i\mu_i + \lambda_a\mu_a\right] \tag{2.12}$$

Thus, the change in current is roughly linearly proportional to the volume that the molecule occupies in the pore, thereby allowing for size interpretation directly from the translocation amplitude. In this regime, the dynamic range of the nanopore sensor is directly related to the volume of the nanopore, with the minimum size being determined by the noise in the current measurement, and the maximum size being determined by the length of the nanopore.

For nanoparticles, viruses, and other analyte molecules whose geometry is fixed, the theory above should provide an adequate first approximation. For polymeric molecules, including DNA and proteins, the conformation of the molecule upon translocation may fluctuate. If, for all conformations the molecule fits entirely inside the nanopore at some point during the translocation event, the signal magnitude is predicted to be independent of the conformation. In reality, there might be some small change in amplitude due to conformational changes. Should this be true, then after multiple measurements, the distribution of translocation amplitudes should be multimodal, and sampled from each of the modes according to the ability of the molecule to change conformations between measurements. However, unless thousands of measurements are performed, it would be difficult to resolve the mean values of modes which differ by a small fraction of the translocation amplitude.

In the case where the length of the nanopore is smaller than the length of analyte as it passes through the nanopore, the analyte length is determined by the translocation duration, τ as:

$$l = \int v_a dt = \int (\bar{v}_a + \delta v_a)\, dt \tag{2.13}$$

$$l \approx \bar{v}_a \tau = \mu_a E \tau \tag{2.14}$$

Equation 2.14 demonstrates that noise in the length measurement in this regime is dependent only upon fluctuations in the analyte velocity, and not the ionic velocity. This is a fundamental difference between the two sizing regimes. Experimentally observed variance in the translocation duration is much higher than would be predicted from thermal fluctuations in the analyte velocity about its mean, in particular due to DNA-pore interactions. Consequently, equation 2.14 does not even provide the correct scaling between size and translocation duration. Wanunu et. al. found instead that the distribution of translocation durations is in fact bimodal, with each mode satisfying $\tau \propto l^n$. They also demonstrated that as the pore diameter decreases from 5 nm and 2.7 nm, the translocation duration increases by orders of magnitude[14]. The bimodal distribution arising from DNA adsorption to the pore is further evidenced in work by Mirsaidov et. al.[15]

Prior experiments therefore suggest that the preferred nanopore geometry for translocation duration sizing is to have a large cross sectional area, and minimum thickness, thereby minimizing analyte pore interactions. When the pore width is more than twice the analyte width, changes in conformation become permissible. Fologea et. al. demonstrated that in the translocation duration regime, the effects of fluctuating conformation can be corrected by instead considering the total electronic charge deficit (ECD) upon

translocation through the nanopore[16]:

$$l \propto \int \Delta I \, dt = ECD \tag{2.15}$$

This statement can be more rigorously derived. Consider the DNA molecule has, at a given instant, a folding multiplicity of $N(t) \in \mathbb{Z}^+$, then the length can be expressed as:

$$l = \int \left(\bar{v}_a + \delta v_a(t)\right) N(t) \, dt \tag{2.16}$$

The folding multiplicity, however, can be determined from the ionic current measurement, $N(I(t))$.

$$\Delta I = eE\Phi N A_a^0 \left[\sum_i \left(\bar{n}_i + \frac{\lambda_a}{z_i}\phi\delta\left(i = i^C\right)\right) z_i\mu_i + \lambda_a\mu_a\right] \tag{2.17}$$

This result therefore means that $\Delta I = \kappa N$, meaning that integral could have been written as:

$$l = \frac{1}{\kappa}\int v_a(t) \, \Delta I(t) \, dt \tag{2.18}$$

$$l = \frac{1}{\kappa} ECD \tag{2.19}$$

At first glance, it seems like the length measurement, would have significant additional noise due to its dependence on the ionic current and the translocation duration. However, since N is an integer, inference on its value can be made with high degree of accuracy provided that the ionic current between $N = k$ and $N = k + 1$ is sufficiently large. Thus, it is perhaps preferable to write the length as:

$$l \approx \bar{v}_a \int N(t)\, dt \tag{2.20}$$

$$l \approx \bar{N}\bar{v}_a\tau = \bar{N}\mu_a E\tau \tag{2.21}$$

Therefore, inference fidelity fundamentally relies on background noise levels and reducing DNA-pore interactions. Since the effects of DNA conformation can corrected for, length measurements on molecules of the same type are in fact improved for larger nanopore cross sectional areas in the limit of thin nanopores provided the translocation event can be detected with high fidelity. The focus of this thesis is on reducing the dominant source of noise at high bandwidths to improve the detection limits using larger cross sectional area nanopores.

2.2 Noise as Derived from Signal Theory

The aim of this section is to develop a model for noise in nanopore devices which can predict noise *a priori* given the ionic concentration, material properties, and device geometry. Noise in this context specifically refers to fluctuations in the measured current. These fluctuations can arise from the physical processes within the nanopore device or within the measurement instrument. The noise model should be able to use the mean field expression for the current through the nanopore device to identify and derive both equilibrium and non-equilibrium noise sources. Since the dominant source of noise is an equilibrium source (see section 2.2.5), derivation of the expression for non-equilibrium noise is beyond the scope of this thesis. However, its origins with respect to the current theory, and its experimental characterization in literature, will be mentioned. Similarly, measurement noise will not be derived here, as it falls more into the purview of am-

plifier design than nanopore physics. Most nanopore sensor experiments use the same measurement instrument, the noise model for the measurement apparatus is already well developed. Here, an estimate of the effect of eliminating the silicon wafer from the device will be presented by through a unified model for noise in nanopore devices. Synthesizing all noise sources into a single equation allows for a comparison of the relative magnitudes of each source.

2.2.1 Mathematical Tools

In practice, all measurements contain within them a measure of uncertainty. This measurement uncertainty, is often referred to as *noise*, and is quantified by the fluctuations of a measurement about its mean, either as the peak to peak fluctuation, or the root mean square fluctuation. In the theory below, we will primarily consider the root mean square fluctuation. Consider a random variable, y, and its Fourier Transform, Y. From Parseval's theorem, we know that the power in the random variable y is equal to the power in its Fourier Transform.

$$\langle y^2 \rangle = \langle Y^2 \rangle \tag{2.22}$$

The average over Y is then written in its integral form as:

$$\langle y^2 \rangle = \int_0^\infty |Y(f)|^2 \, df \tag{2.23}$$

Using this, we define the power spectral density as:

$$S_y(f) = |Y(f)|^2 \tag{2.24}$$

The power spectral density is a measure of the total fluctuations of a parameter

after subtraction of its DC component. In particular, the RMS, δy_{RMS}, noise can be written as:

$$\delta y_{RMS} = \sqrt{\left\langle (y - \bar{y})^2 \right\rangle} = \sqrt{\int S_y(f)\, df} \tag{2.25}$$

If we seek to find the power spectral density of a function, f, which is in fact a function of the variable y in the sense $f = f(y)$, then the power spectral density of f can be written in terms of the power spectral density of y:

$$S_f = \left(\frac{\partial f}{\partial y}\right)^2 S_y \tag{2.26}$$

Equation 2.26 is the means by which the signal theory derived above will be used to understand the origins of noise. The ionic current through the nanopore is a function of the electric field, the geometry of the analyte, the concentration of ions, the electrophoretic mobility of the ions and analyte, and the Manning-Oosawa condensation factor, the charge of the ions and analyte. It is assumed, however, that fluctuations in the applied voltage from the Ag/AgCl electrodes are minimal, and that the geometry of the nanopore is constant. Thus fluctuations in the electric field are caused only by fluctuations in the charge density (as $\nabla \cdot \vec{E} = \rho/\epsilon$). In the case where there is no significant free charge polarization, the electric field fluctuations transverse to the nanopore cross section are likely to be relatively small compared to the electric field through the nanopore. Furthermore, the geometry of the analyte and the charge of each ion and analyte are assumed to be constant. Thus, it is expected that fluctuations in the total ionic current can be expressed in terms of fluctuations in ion concentration (number density) and electrophoretic mobility.

2.2.2 Equilibrium Current Fluctuations

The aforementioned mathematical relationships were expressed in particular because the power spectral density of a variable is a convenient tool for the analysis and understanding of noise sources. Fluctuations in the ionic current, though, fundamentally arise from statistical mechanics. The two dominant sources of ionic current fluctuations are velocity fluctuations and number of ion fluctuations. Velocity fluctuations can be divided up into equilibrium (thermal: resistive and capacitive) fluctuations and non-equilibrium (mobility) fluctuations. Number fluctuations are also a source of non-equilibrium noise which follow the same scaling as mobility fluctuations. From equation 2.1 and 2.26, the contribution of velocity fluctuations can be expressed as:

$$S_I = \sum_{j\ s.t.\vec{x}_j \in V} e^2 z_j^2 S_{v_j} \tag{2.27}$$

Converting to the sum over all ionic species yields:

$$S_I = \sum_i n_i e^2 z_i^2 S_{v_i} \tag{2.28}$$

To progress further with the interpretation of current fluctuations, the PSD of the velocity of each species is expressed explicitly. For convenience, the subscript referring to the species type is henceforth dropped, but will be added when computing the total PSD of the current. Using the Wigner-Khinchine theorem:

$$S_{\Delta v} = \int v\,(t)\, v\,(t+s)\, ds \tag{2.29}$$

The frequency dependent In equilibrium, van der Ziel derives the relationship between the PSD of the velocity fluctuations and the diffusivity[17]:

Variable	Symbol
V	Represents volume of nanopore
S_I	Power spectral density (PSD) of current
S_{v_i}	PSD of the velocity of the i^{th} species
$S_{\bar{n}_i}$	PSD of the mean number density of the i^{th} species
$D(f)$	Frequency dependent diffusivity

Table 2.2: Variables for Nanopore Noise Theory

$$S_{\Delta v}(f) = 4D_{eq}(f) \tag{2.30}$$

Using Einstein's fundamental relationship, the diffusivity can be related to the mobility, $D(f) = \frac{k_b T}{ze}\mu$:

$$S_I(f) = 4k_b T \sum_i e z_i n_i \mu_i(f) \tag{2.31}$$

The sum, $\sum_i e z_i n_i \mu_i$ is now recognized to be the frequency dependent conductivity $g(f)$, or equivalent admittance of the circuit, $Re[Y(f)]$, thereby obtaining the equation for equilibrium current fluctuations:

$$S_I = 4k_b T\, Re(Y_{eq}) \tag{2.32}$$

The equilibrium noise is thus a function of the equivalent admittance of the device. Consider now a circuit model of a nanopore with a single resistor with Y_R(nanopore) in parallel with a leaky capacitor (lumped constant phase element for the silicon wafer and the membrane) with Y_C. Since the admittance of circuit elements in parallel add directly, the total equilibrium noise can be written as:

$$S_I = 4k_b T\,[Re(Y_R) + Re(Y_C)] \tag{2.33}$$

$$S_I = S_R + S_C \tag{2.34}$$

Thus, the total equilibrium noise can be divided up into a contribution from the nanopore resistance alone, and a contribution from the leaky capacitor in parallel with the nanopore. Estimates for the capacitance, C and dissipation factor, D of the leaky capacitor in parallel with the nanopore for state of the art nanopores can be found in literature [9, 10]. Thus, the RMS noise from the nanopore resistance is calculated by performing the integration of S_R as defined by Equation 2.25:

$$\delta I_R = \sqrt{4k_bT\,B/R} \tag{2.35}$$

Where B is the analog filter bandwidth. Using the admittance of a leaky capacitor to perform the integration of $S_C = 4k_bT\,Re\,(Y_C)$, the contribution to the noise from the leaky capacitor is:

$$\delta I_C = \sqrt{4k_bT\,C\,D\,B^2} \tag{2.36}$$

2.2.3 Non-Equilibrium Current Fluctuations

There are two predominant sources of non-equilibrium current fluctuations in the absence of analyte molecules. The first arises from non-equilibrium contributions to the velocity fluctuations, S_{v_i}. These fluctuations cause the diffusivity, D to differ from the equilibrium diffusivity, D_{eq}. Typically, these fluctuations are described by passing them over to the electrophoretic mobility through the Einstein relationship.

The other source of non-equilibrium noise arises from fluctuations in the number of ions which the sum runs over. It is likely that the dominant source of these number fluctuations is the generation and recombination of ions at the nanopore surfaces. As

presented here, both of these non-equilibrium fluctuations should satisfy Hooge's phenomenological relationship[17]. See van der Ziel's book, *Noise in Solid State Devices and Circuits* for the derivation for Hooge's relationship as it arises from non-equilibrium resistance fluctuations (mobility and number density fluctuations). Experiments in nanopore devices have verified that flicker noise flicker noise (whose spectral density decays as $1/f$ does indeed follow Hooge's relationship [10, 18].

$$S_I = \frac{\alpha I^2}{N_C f} \tag{2.37}$$

Where α is a device constant called Hooge's parameter, N_C is the number of charge carriers in the device, and f is of course the frequency. From prior experiments, an estimate for the value of α can be obtained, and therefore, the contribution of non-equilibrium flicker noise can be estimated. The noise contribution from flicker noise is:

$$\delta I_F = \sqrt{\frac{\alpha I^2}{N_C} ln\,(B)} \tag{2.38}$$

2.2.4 Measurement Noise

So far, contributions to the noise arising from current fluctuations in the nanopore have been considered. A non-trivial component of the noise, however, arises from the measurement instrument itself. In our experiments, the Axopatch 200B (Molecular Devices Inc.) is used to perform current measurements and apply a voltage. Uram et. al. investigated noise from the amplifier and developed a model for it[19]:

$$\delta I_M = \sqrt{2qI_{fet}c_1 f_c + \frac{4ak_B T_h c_1 f_c}{R_f} + e_n^2 \left(\frac{c_1 f_c}{R_f^2} + \frac{4}{3}\pi^2 C_t^2 c_3 f_c^3 \right)} \tag{2.39}$$

The first term, $2qI_{fet}c_1 f_c$ represents the shot noise due to the current passing through

Variable	Symbol
I_{fet}	Current through the Field Effect Transistor in the headstage
c_1	Constant of integration from 8 pole Bessel filter
T_h	Headstage temperature
f_c	Cutoff frequency for Bessel filter
e_n	Input voltage fluctuations to the feedback loop in the amplifier
R_f	Resistance in the feedback RC circuit in the amplifier
C_t	Total capacitance of the feedback RC circuit in the amplifier

Table 2.3: Variables for Current Modulation Theory

the field effect transistor in the amplifier. The second term, $\frac{4ak_BT_hc_1f_c}{R_f}$ arises from equilibrium current fluctuations through a specific resistor (the feedback resistor) in the circuit. Finally, the third term, can be understood by considering voltage fluctuations, $S_V = e_n^2$ which are input into an RC circuit. Using Ohm's law, $I = VY$, and equation 2.26, the expression $e_n^2\left(\frac{c_1f_c}{R_f^2} + \frac{4}{3}\pi^2C_t^2c_3f_c^3\right)$ is obtained.

Values for the parameters in the measurement noise formula found in literature were verified using high quality resistors.

2.2.5 Noise Estimates

Assuming that each of the noise sources above is independent of each other, the total noise can be calculated by adding each noise source in quadrature:

$$\delta I = \sqrt{\delta I_F^2 + \delta I_R^2 + \delta I_C^2 + \delta I_M^2} \tag{2.40}$$

Since the values of each of the relevant parameters for the current state of the art nanopore devices have been reported in literature, it becomes possible to plot the total noise as a function of bandwidth and simultaneously estimate the contributions of each noise source to the total noise, as in Figure 2.1. For these estimates, a nanopore resistance of 30 MΩ has been used, with an exposed membrane area of 100 μm $\times$ 100

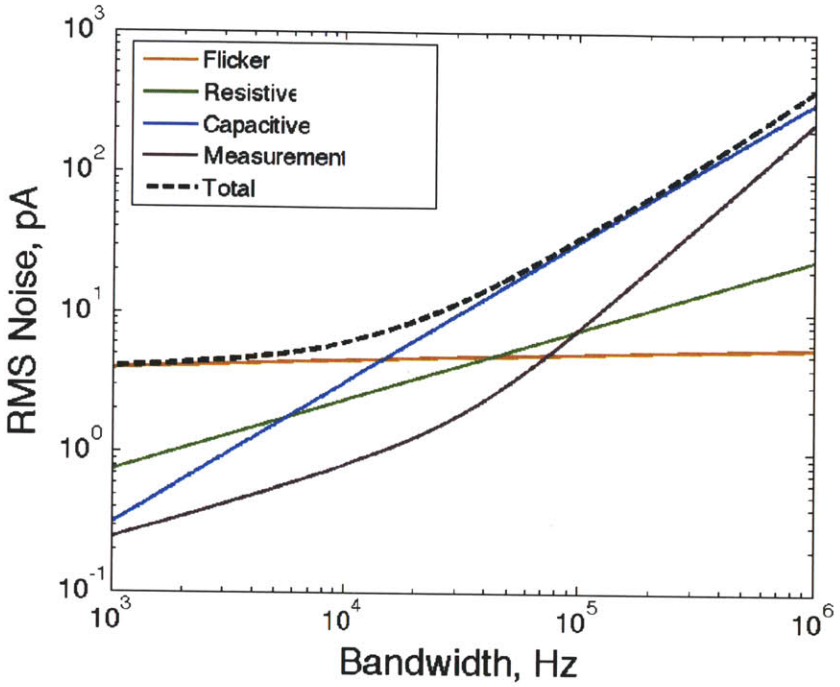

Figure 2.1: Noise Estimates in Typical Solid State Nanopore

μm, and a thickness of 50 nm. Parameters for the capacitance noise, flicker noise, and measurement noise were taken or extrapolated from literature[10, 18, 9, 19].

The noise estimate demonstrates that the dominant source of noise at the target bandwidth of 100 kHz is capacitive noise. The dominant contribution to the capacitive noise arises from the silicon wafer handle associated with the membrane. Therefore, we reasoned that removal of the silicon wafer handle would significantly reduce the capacitance, and thereby greatly decrease the total capacitive noise.

Chapter 3

Multiple Measurements and Recapture Probability

Historically, the most common method for improving the precision of a measurement has been to repeat the measurement. With only a single measurement, the uncertainty (standard deviation) in the mean is the RMS noise, σ_0. After repeating the measurement multiple times, the standard deviation of the set of N measurements tends to converge to the RMS noise, while the standard deviation in the mean (SDOM) scales as: $\sigma_N = \sigma_0\sqrt{N}$ (for a Gaussian distribution).

In nanopore sensors a single measurement corresponds to one translocation event. Consequently, to perform N measurements on the same molecule, the molecule must translocate through the nanopore N times. One method for performing such measurements is to use a feedback control algorithm to reverse the voltage bias each time the analyte molecule translocates through the nanopore. Once the voltage is reversed, the DNA molecule electrophoretically migrates back towards the nanopore while simultaneously randomly diffusing. The technique is schematically illustrated in Figure 3.1. Feedback control for repeatedly measuring the same analyte through a constriction was

first performed in Coulter counters in 1989[20]. The technique was then applied to nanopore sensors in 2007 by Gershow et. al. [12]. In Gershow et. al.'s work, the experimentally measured probability for DNA recapture was in good agreement with probabilities predicted from a simple drift-diffusion model for DNA transport. The electric field strength outside the nanopore, however, decayed sufficiently fast that recapture probabilities were fairly low. The goal here is not to present full and detailed solutions of the Poisson-Nernst-Planck equation and then the diffusion-convection equation in 3D for the resultant DNA recapture probabilities. Rather, the aim is to show that the electric field can be confined using microchannels, and to demonstrate the benefits of electric field confinement using microchannels outside of the nanopore.

The device design presented in the introduction contained microchannels on either side of the nanopore. The electric field profile outside of the nanopore is therefore defined by the geometry of the nanopores. COMSOL simulations of the electric field profile will be presented. Most importantly, the microchannels act to confine the electric field, thereby increasing the probability of recapture. Furthermore, assuming a square cross section, the electric field becomes nearly one dimensional one channel width upstream/downstream of the nanopore. Consequently, the drift-diffusion equation will be solved in one dimension, and the recapture time (time prior to analyte translocation with greater than 99.99% probability) will be obtained. This expression should be valid if electro-osmotic flow is negligible. One method for ensuring that this criterion is met may be to use surfactants such as polyvinylpyrollidone [21].

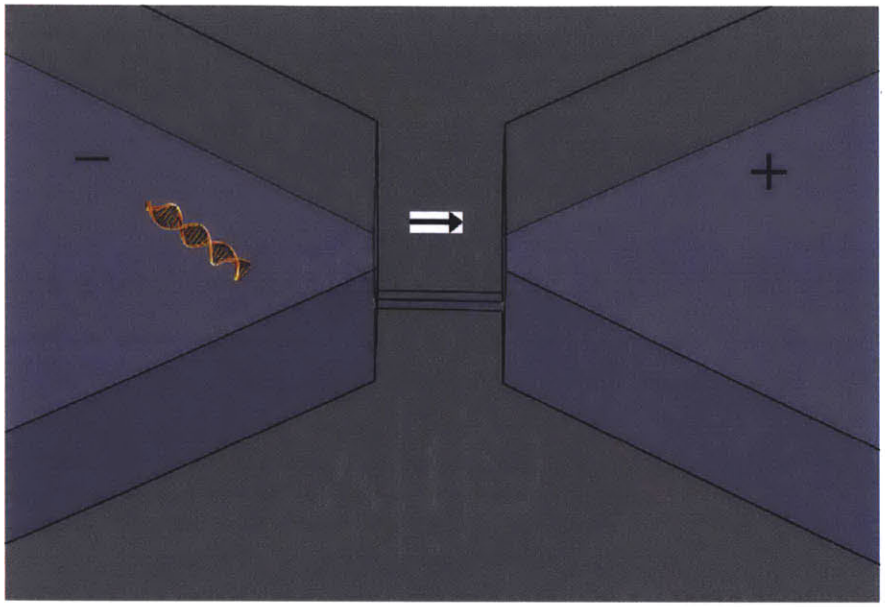

(a) DNA and applied voltage after even number of translocations (0,2,4,...)

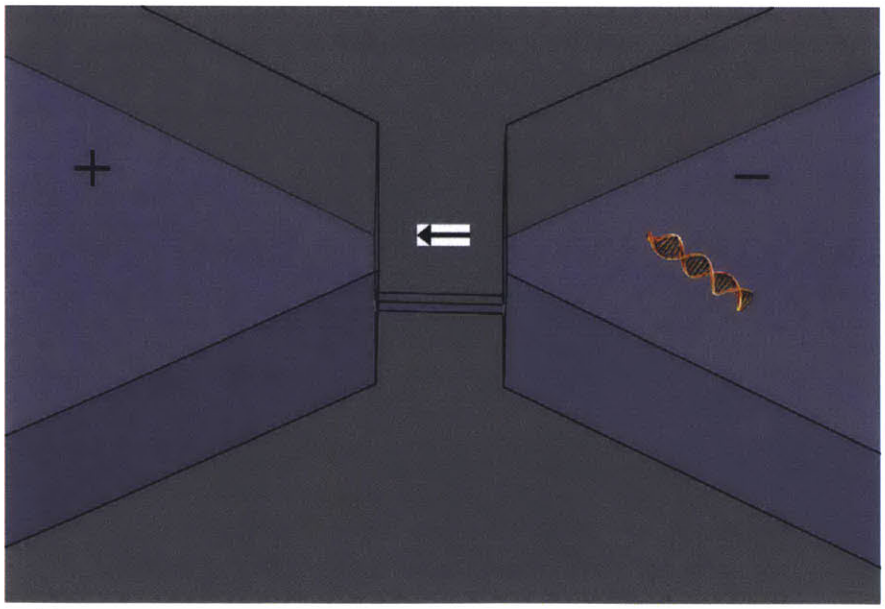

(b) DNA and applied voltage after odd number of translocations (1,3,5,...)

Figure 3.1: Illustration of feedback control for performing multiple measurements.

Condition	Interpretation
$x = 0$	Location of nanopore
t_p	Time after translocation prior to reversal of voltage
t_r	Time to achieve 99.99% recapture probability
$x_0 = \mu E t_p + 2\sqrt{D t_p}$	Initial position of DNA
$C(x, t = 0) = \delta(x = x_0)$	Initial probability distribution of DNA
$C(x \to \infty, t) = 0$	Boundary condition at ∞
$C(x \to -\infty, t) = 0$	Boundary condition at $-\infty$
$p_r(t)$	Recapture Probability
ΔV	Voltage drop over microchannel

Table 3.1: Boundary Conditions, Initial Conditions, and Variables for 1D Recapture Model

3.1 Recapture Probability: 1D

Here, the one-dimensional recapture probability is studied using the drift-diffusion equation, which a partial differential equation expressing conservation of mass. In this case, the concentration, C can be interpreted as the probability of finding the DNA at a specific location. Therefore, the integral of C will be normalized to 1 at the starting point.

$$\frac{\partial C}{\partial t} = D\frac{\partial^2 C}{\partial x^2} - \mu E\frac{\partial C}{\partial x} \tag{3.1}$$

The boundary conditions and initial conditions for this PDE were used as shown in Table 3.1:

A rigorous treatment of the problem would require that that the drift diffusion equation be solved prior to voltage reversal in order to obtain the initial condition for the drift diffusion equation after voltage reversal. This would mean that the initial condition at $t = 0$ (right after voltage reversal) would not be a delta function, but some distribution about the mean DNA travel distance of $\mu E t_p$ during the pre-reversal time. In order to simplify the problem, the initial condition right after voltage reversal was

estimated as a delta function instead of the distribution from solving the drift-diffusion equation. However, in order to compensate for this approximation, two standard deviations, $2\sqrt{Dt_p}$ of the the actual initial position distribution were added to the mean DNA travel distance. The delta function at $x_0 = \mu E t_p + 2\sqrt{Dt_p}$ therefore overestimates the initial position of roughly 97.7% of the initial position distribution.

The probability of recapture in this model is expressed as:

$$p_r(t) = \int_{-\infty}^{0} C(x,t)\, dx \tag{3.2}$$

In this expression for the recapture probability as a function of time, the nanopore is considered to be at the position $x = 0$. Probability of finding the molecule at $x < 0$ is taken to mean that the DNA would have translocated. A more realistic treatment of the nanopore in the equation would have been to introduce a probability sink at $x = 0$. This would, however, be likely to increase the overall recapture probability compared to the current method of calculating the recapture probability. Thus, the mathematical formulation of the initial condition and recapture probability not only greatly simplify analytic calculation, but provide *conservative* estimates. The solution to the drift diffusion equation, is found to be:

$$C(x,t) = \frac{1}{\sqrt{4\pi Dt}} e^{-(x-x_0-\mu Et)^2/4Dt} \tag{3.3}$$

From this, the recapture probability is:

$$p_r(t) = \frac{1}{\sqrt{4\pi Dt}} \int_{-\infty}^{0} e^{-(x-x_0-\mu Et)^2/4Dt} dx \tag{3.4}$$

Successive change of of variables 1) $y = x - x_0$ and then 2) $\xi = \frac{y-\mu Et}{\sqrt{2Dt}}$ yields:

$$p_r(t) = \frac{1}{\sqrt{4\pi Dt}} \int_{-\infty}^{-x_0} e^{-(y-\mu Et)^2/4Dt} dy \tag{3.5}$$

$$p_r(\xi_0) = \int_{-\infty}^{-\xi_0} \frac{1}{\sqrt{\pi}} e^{-\xi^2} d\xi \tag{3.6}$$

Where $\xi_0 = \frac{x_0+\mu Et}{\sqrt{2Dt}}$. This integration is analytically performed and equal to:

$$p_r(t) = \frac{1}{2} erfc\left(\frac{x_0 + \mu Et}{\sqrt{2Dt}}\right) \tag{3.7}$$

Provided that the Peclet number (with the relevant lengthscale being the microchannel length, L), $Pe = \frac{\mu EL}{D} = \frac{\mu \Delta V}{D} > 1$, the one dimensional drift diffusion equation has the property that the distribution translates faster than it spreads. However, it is only when $Pe \gtrsim 100$ that the recapture time t_r is sufficiently small for this methodology to be useful in nanopore devices. In particular, the relationship between the Peclet number and the recapture time is depicted in figure 3.2. The other requirement is that the microchannel should be long enough so that the molecule does not leave the microchannel during the pre-reversal time t_p.

In order to appropriately apply this model:

1. The electric field must be approximately 1D in the region of application
2. The correct magnitude for the electric field must be obtained for the given microchannel geometry

Provided that the microchannel width and height are small compared to its length, the electric field will likely become one dimensional. In this regime of microchannel geometries, the resistance of the microchannel, the nanopore, and Ohm's law can be

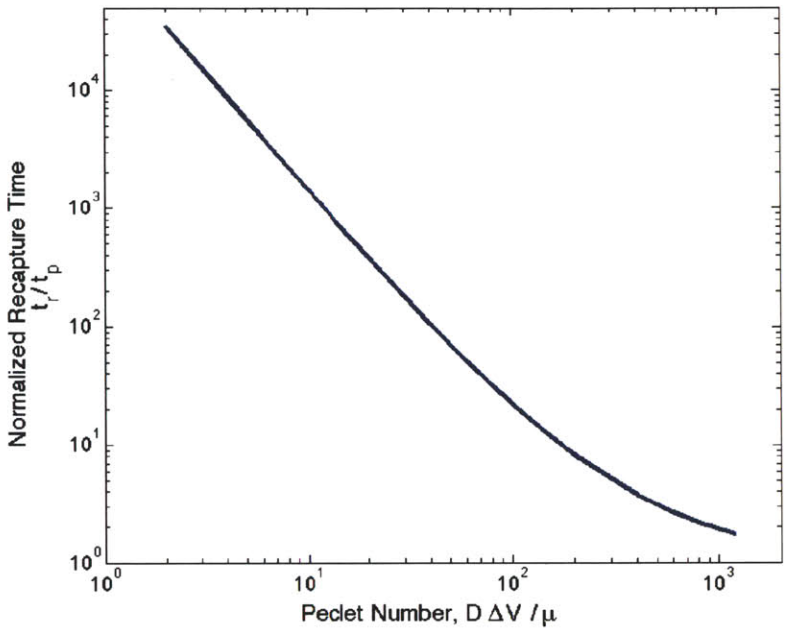

Figure 3.2: Relationship between the dimensionless recapture time (normalized by the pre-reversal time) and the Peclet number for the one dimensional model

used to obtain a rough estimate for the electric field once it becomes one dimensional. In order to obtain the actual electric field, finite element simulations were performed.

3.2 Simulations of Electric Field

In the absence of free charge polarization within the region of interest, the charge density, $\sum_i \rho_f^i$ is zero, and the electric field is completely specified by the geometry and the applied voltage:

$$\nabla^2 V = \nabla \cdot \vec{E} = 0 \tag{3.8}$$

The electric field in the entire system was computed numerically using finite elements methods (COMSOL) to solve the PDE above. The initial geometric configuration is

Geometric Parameter	Value
Nanopore Diameter	12.5 nm
Nanopore Length	$100nm$
Microchannel Width	$2\mu m$
Microchannel Height	$1\mu m$
Microchannel Length	$10\mu m$

Table 3.2: Initial Geometry for Electric Field Simulations

displayed in table 3.2. Only half of the device (from the nanopore midpoint to the end of the microchannel) was simulated. For a total applied bias of 1 V, the voltage at the nanopore midsection must by symmetry be 0.5 V. The voltage was set to 0 at the end of the microchannel.

Close the the nanopore, the electric field decays at the same rate as it would have without the confining microchannels. Figure 3.3b presents graph of the voltage decay as a function of distance from the nanopore, demonstrating the initial r^{-2} decay followed by a tapering off to a near constant value within a distance slightly smaller than the microchannel width. This transition from 3D to 1D is further visualized in Figure 3.4a. The transition from 3D to 1D at roughly the microchannel height was tested across geometries where the height to width ratio was no more than 2 or less than 1/2. One would expect that if the microchannel cross section had one dimension significantly larger than the other, then the electric field would first become two dimensional before reducing to one dimensional. For lengthscales smaller than the microchannel height, the three dimensional recapture theory using the drift diffusion equation should be considered.

By varying the geometry of the nanopore and microchannel, the following observations were verified. The electric field strength inside the nanopore, to within several percent, could be approximated by dividing the applied voltage by the nanopore length. The terminal electric field in the microchannel could also be approximated similarly by

modeling the microchannel as a resistor in series with the nanopore to within roughly 10%. Furthermore, the electric field strength in the microchannel is predominantly a function of the cross sectional area, and is only a weak function of the length.

Gershow et. al. [12] constructed a lengthscale comparing the mobility and diffusivity, called the recapture radius, to qualitatively express the radius of capture in three dimensions. This lengthscale was given as:

$$r_{recap} = \frac{\mu I}{2\pi\sigma D} \tag{3.9}$$

Where σ is the conductivity of the fluid. When the recapture radius in 3D is larger than the microchannel width, and the constant 1D electric field in the microchannel provides a sufficiently large Peclet number (as presented above), then the effect of one dimensional confinement is to create a near infinite recapture radius. Electrophoretic mobility is independent of DNA length, and close to $\mu = 4.1 \times 10^{-8} m^2/V\,s$ in free solution, while the diffusivity is a function of length[22]. For 1 kbp DNA, the diffusivity is roughly $2 \times 10^{-11} m^2/s$[22]. For given analyte mobility and diffusivity, the recapture radius can be tailored to a value above the microchannel width by either increasing the total current through the nanopore or decreasing the conductivity of solution.

3.2.1 Assumptions

At this time, it is imperative to recollect the fundamental assumptions made in this theory. First, free charge polarization has been ignored. The dominant cause of free charge polarization is the presence of surface charge on both the nanopore and the microchannels. Second order corrections to the electric field can be calculated by solving

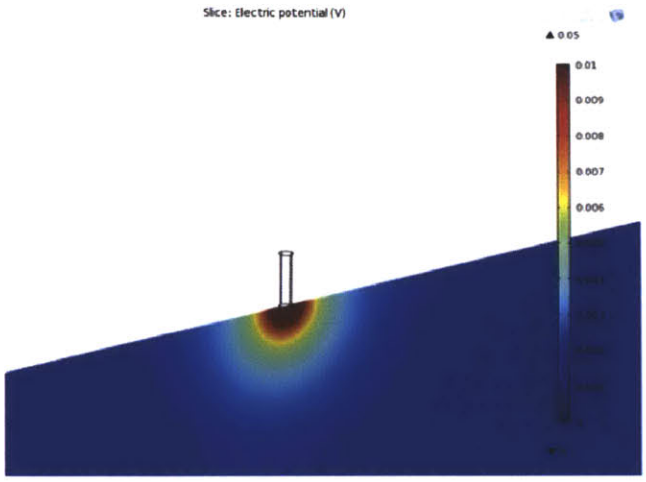

(a) Voltage cross section around nanopore

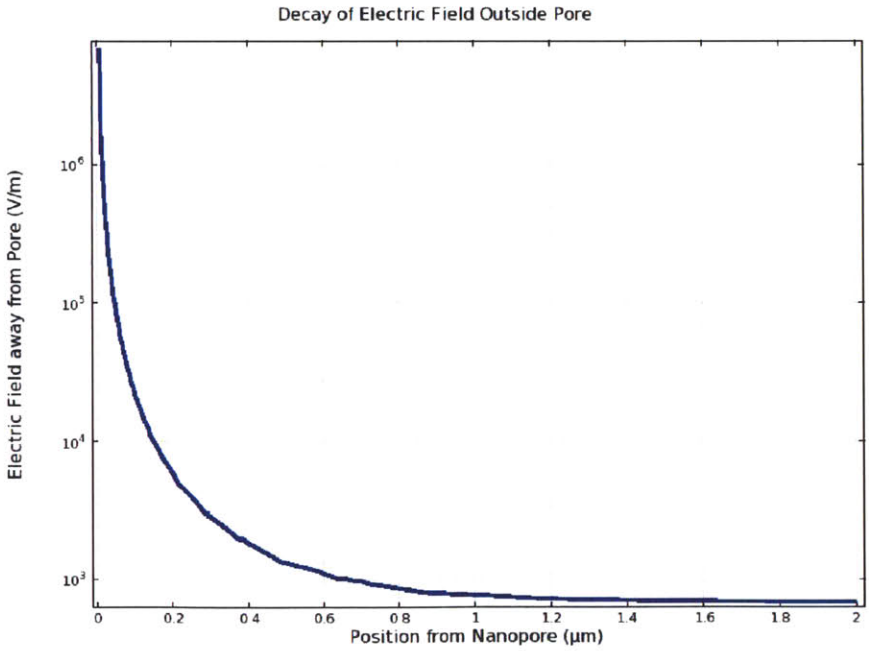

(b) Electric field along length of the microchannel, starting from the nanopore

Figure 3.3: Electrostatics COMSOL simulations, I

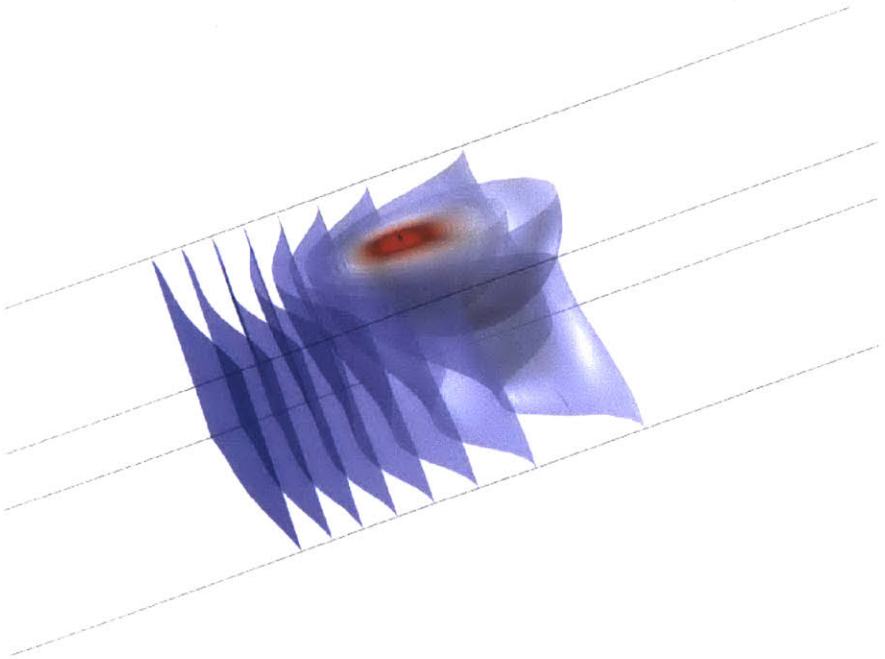

(a) Transition of electric field from 3D to 1D

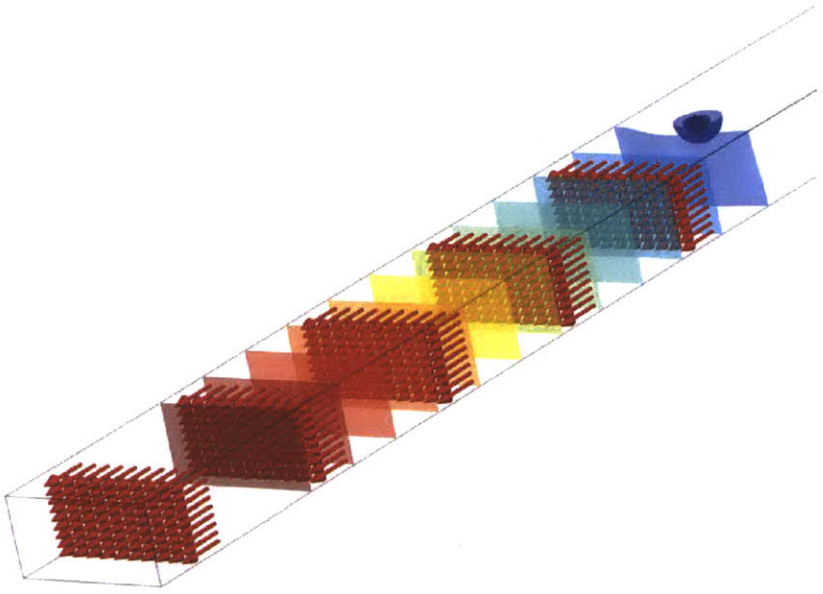

(b) Graphical illustration of one dimensional electric field

Figure 3.4: Electrostatics COMSOL simulations, II

the Poisson-Boltzmann distribution for the charge distribution from the surface charge, and then superimposing it onto the electric field from the applied voltage. The free charge in solution has the effect of screening the surface charge. In the case that the Debye length, $\lambda = \left(\frac{\epsilon_r \epsilon_0 k_B T}{\sum_i n_i^0 z_i^2}\right)^{1/2}$ is significantly smaller than the microchannel dimensions, the contributions of the surface charge to the drift velocity of the analyte (directly through the electric field) can be ignored, and electroosmotic flow can be approximated as a simple plug flow in the microchannel. If a surfactant is used to suppress electroosmotic flow, even that effect can be ignored. In the case where the Debye length is a non-trivial fraction of the microchannel width, the full Poisson-Nernst-Planck equations would need to be solved to obtain the flow profile and the resultant electric field.

Chapter 4

Nanopore Fabrication

4.1 Current Fabrication Methods

The predominant method of solid state nanopore fabrication is to use collimated electron or ion beams accelerated by tens of thousands of volts. Typically, the beam of ions or electrons sputters atoms from the substrate upon impact. Storm et. al. found that prolonged exposure to a high voltage (200 kV) electron beam reduces the diameter of the nanopore at a slow and controllable rate[23]. In a TEM, the simultaneous ability to image the nanopore thereby allows for nanometer precision on nanopore diameters. Focused ion beam sculpting, is a similar technique developed by Li et. al., whereby ion beam induced lateral mass flow causes a decrease in the nanopore diameter. The final diameter is controlled by using feedback control on the ion current through the membrane during nanopore fabrication[24]. Of these two methods, TEM fabrication is the method of choice, as it creates nanopores with a more preferred geometry (hourglass instead of conical) and allows for direct visualization of the sub-nanometer structure of the nanopore. A recent study by van den Hout et. al., however, suggests that optimal nanopore stability is achieved when the nanopore diameter is as close as possible to the

electron beam diameter[25].

The search for cheaper and high throughput nanopore fabrication methods have led to the development of some of notable alternatives. Spinney et. al. used water vapor assisted focused electron beams (< 20 kV) to produce nanopores with diameters down to 5 nanometers[26]. Menard et. al. deposited a 100 nm sacrificial chromium layer over the silicon nitride membrane prior to nanopore fabrication with a focused ion beam. Since the sputtering rate of chromium is lower than silicon nitride, the layer acts as a partial mask to the ion beam during fabrication, thereby allowing for fabrication of line-widths down to 5-10 nm [27]. Atomic layer deposition has been used by Chen. et. al. to shrink the diameter of larger nanopores[28]. Since the the growth of ALD films is self-limited to a layer by layer process, the growth rate is slow, repeatable, and high throughput.

Due to some of the design considerations (which will be discussed in chapter 5), a process which permitted high-throughput fabrication of 10-15 nm diameter nanopores was required. The simplest method was to use a focused ion beam to create larger nanopores, and then use ALD to shrink the nanopores down to the desired diameter. In this chapter, the details of nanopore fabrication will be discussed.

4.2 Focused Ion Beam Nanopore Fabrication

4.2.1 Important Parameters

Without reliance on nanopore shrinking methods, the beam spread determines the lower limit on the possible nanopore size that can be obtained. For this reason, both high accelerating voltage and small beam currents provide optimal milling resolution. On the equipment used (Helios 600 Dualbeam, FEI Company), the maximum accelerating voltage was 30 kV. The smallest beam currents available were 1.5 pA or 9.7 pA. Obtaining

minimal pore size and circular cross sections require accurate focusing of the ion beam optics and appropriate astigmatism correction respectively. Due to the non-conducting nature of the silicon nitride substrate, however, such calibration is often quite difficult. These challenges are accentuated as the beam current decreases, as imaging contrast (and consequently the ability to align and focus the ion beam optics) decreases with decreasing ion beam voltage. Therefore, we investigated the fabrication of nanopores at the second lowest beam current of 9.7 pA as well as the lowest beam current of 1.5 pA. Figure 4.1 provides an example of a nanopore generated with an incorrectly stigmated ion beam at 1.5 pA, thereby demonstrating the importance of correctly calibrating the ion beam.

4.2.2 Experimental Data

In order to determine the optimal dose for nanopore milling, a circular array of nanopores was made in a silicon nitride membrane. The dose was varied as a function of the radius, (Figure 4.2). To make each nanopore, the ion beam exposes a single point for a specified amount of time. During this time, the beam is not moved or rastered, but stays fixed. Therefore, the relevant parameter describing the ion beam dosage is the total number of ions incident on the surface, and not the incident charge density. The actual nanopore diameters were measured in a transmission electron microscope. A 5 μm hole was made in the center of the circular array as an easily identifiable detection mark in the TEM. The nanopore diameter as a function of dose is presented in Figure 4.3. The results are in close agreement to the calibration curve measured by Schiedt et. al. in SiN_x membranes of the same 50 nm thickness (although the equipment we used was different)[29]. Figure 4.4 shows TEM images of the nanopores above.

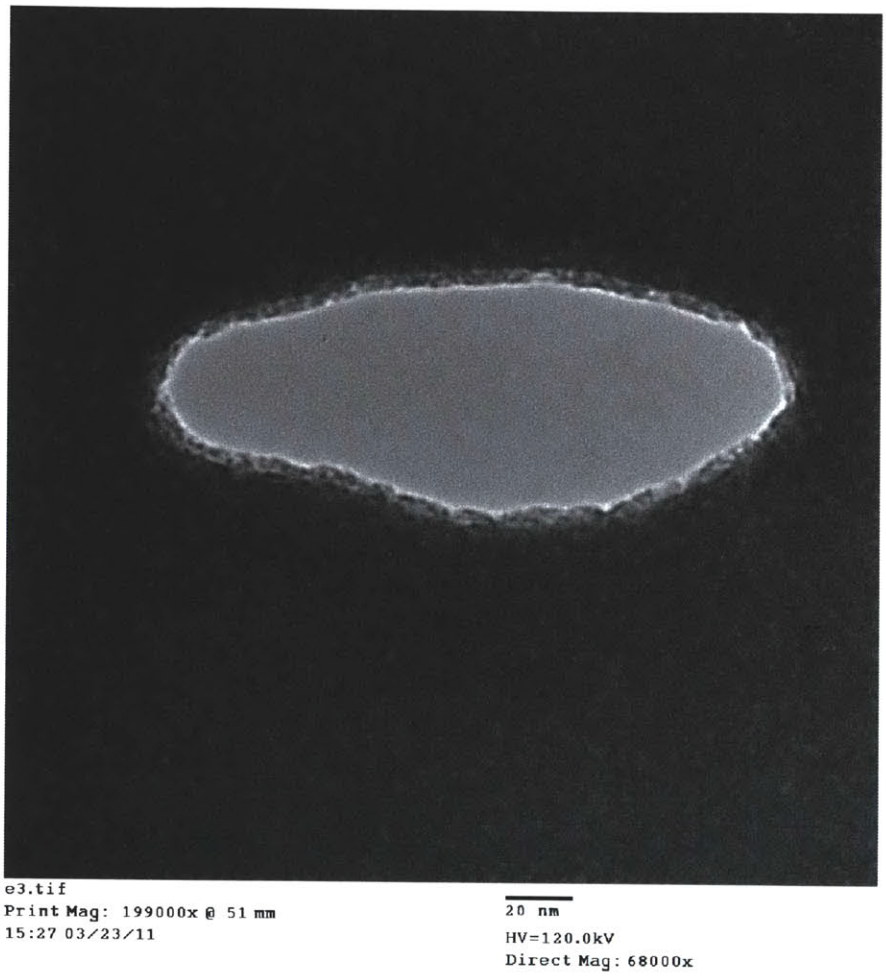

Figure 4.1: TEM Image of a nanopore made with a highly astigmated ion beam at 1.5 pA and 30kV accelerating voltage.

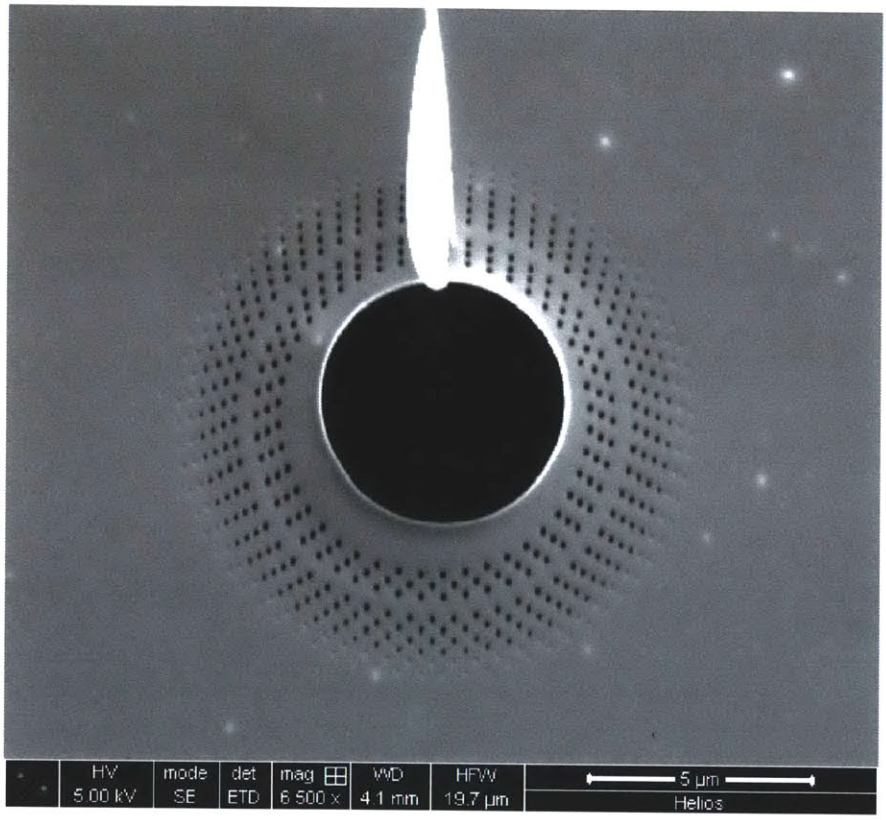

Figure 4.2: SEM image of nanopore array with radial variation in dose.

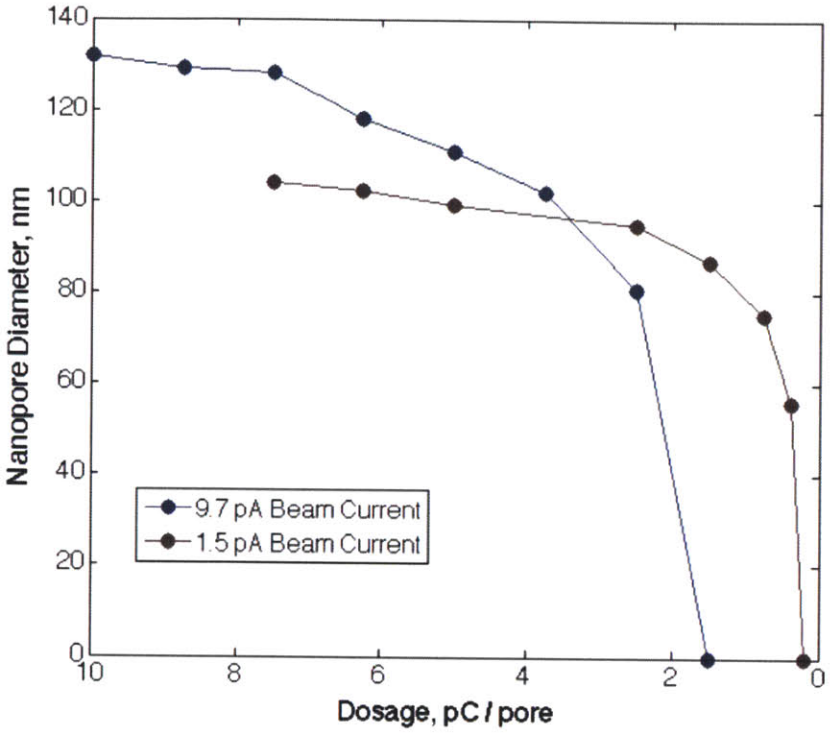

Figure 4.3: Nanopore size calibration data

The nanopore size calibration data clearly shows that there is a critical dosage above which the nanopore formation begins. The rapid increase in nanopore diameter with increasing dose right after nanopore formation suggests that the nanopore shape is initially conical. When the slope tapers off, at about 80 nm diameter for 1.5 pA, and 100 nm for 9.7 pA, the nanopore geometry is expected to be only slightly conical. According to equipment specification, the beam diameter is roughly 5 nm, which is much smaller than the pore sizes observed. Deeper investigation into the physical origins of

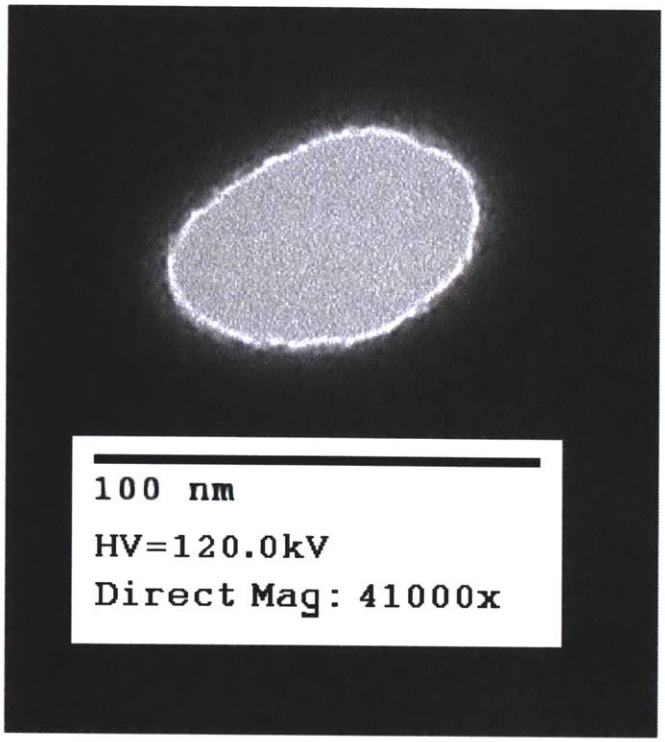

(a) Nanopore made using 1.5 pA beam current

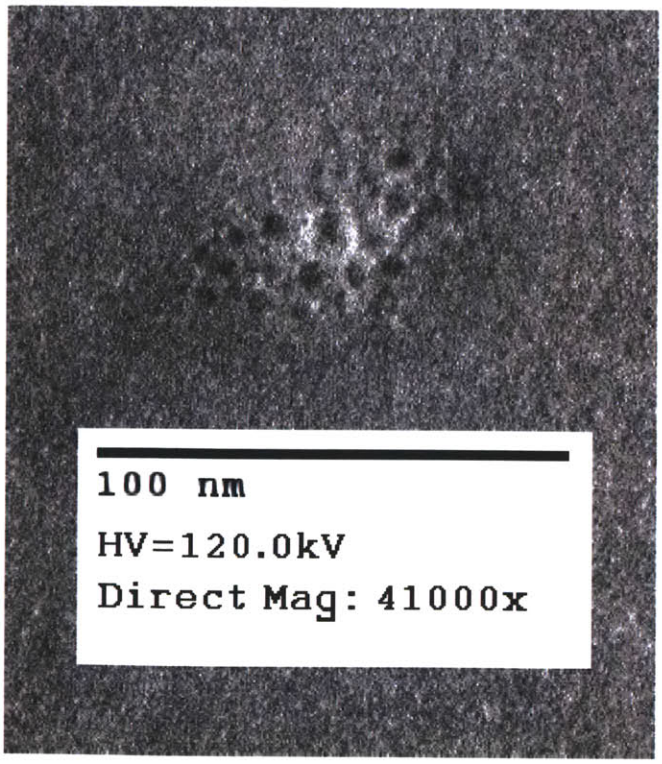

(b) Nanopore prior to milling completely through membrane using 1.5 pA beam current

Figure 4.4: TEM Images of nanopores made with 1.5 pA beam current at 30 keV

the multiple peaks and valleys in image intensity (Figure 4.4) would perhaps aid in creating smaller nanopores directly with a focused ion beam. To obtain the desired nanopore diameter, atomic layer deposition was performed. The number of cycles of ALD growth is determined after measurement of the nanopore diameter with a TEM after FIB fabrication.

Chapter 5

Device Design and Fabrication

The fundamental physical principles presented in the previous chapters demonstrate that the concept of transferring a membrane between two perpendicular microchannels poses significant advantages towards improving the resolution of nanopore sensors. The theory, however, imposes predominantly geometric constraints on the device, whose realization requires:

1. A method for alignment of the nanopore over the microchannel
2. A method for *high yield* removal of the membrane from its silicon backing and onto a substrate with a microchannel

These two *Fundamental Constraints* will be addressed in the this chapter. Provided that these two criterion are satisfied, there exists some flexibility concerning the choice of materials, the nanopore fabrication process, and the device assembly process. To address these degrees of freedom, additional *Design Constraints* were added. These constraints were chosen such that future implementation of the device concept is facilitated :

1. Allows for ease of integration with, and rapid prototyping of, the microfluidic

system connected to the microchannels encapsulating the nanopore

2. Tools used for fabrication process should enable wafer scale fabrication of nanopore devices with minimal cost and number of fabrication steps

5.1 Alignment of Nanopore Over Microchannel

Since the nanopore is too small to be optically resolved in a substrate alignment process, the most obvious method for aligning the nanopore with the microchannel would be to fabricate alignment marks in the free standing membrane prior to nanopore fabrication. These alignment marks would serve to indicate where the nanopore should be made with the electron or ion beam, and could also then be used as alignment marks for the alignment between the membrane and the microchannel substrate. Such alignment marks could be made either using photolithography or focused ion beam milling.

An alternative method for alignment of the nanopore over the microchannel would be to create a square array of nanopores with a pitch equal to the microchannel spacing. Provided that the tolerance for the angular alignment between the microchannel and free-standing membrane is met, this method removes the need to make alignment marks, and also increases the spatial alignment tolerance from the width of the microchannel to the width of the free-standing membrane. Since the membrane width must always be greater than the microchannel width, this technique offers significant improvements in alignment tolerance.

However, this method also requires that an array of nanopores be made in lieu of alignment marks. The choice of alignment method therefore depends on the method which is used to fabricate the nanopores. Due to the ease of alignment, the devices fabricated in this thesis were made with an array of nanopores. In a Focused Ion Beam (FIB), such an array of nanopores can be made in several minutes. Instead of

fabricating devices on a silicon wafer, 3mm TEM grids with 50 nm of SiN_x deposited using low pressure chemical vapor deposition (LPCVD). The free-standing membrane SiN_x membrane in these grids was 100 μm $\times$ 100 μm, and with the square array of nanopores, the membrane alignment tolerance was roughly $\pm$ 30 μm $\times$ 30 μm.

In order to perform the nanopore alignment with the microchannel, a custom grid aligner was constructed. The TEM grid aligner consists of a three axis micropositioner placed on top of the stage of a transmitting light microscope. The micropositioner is held in place using a magnetic base. A vacuum pen attached to the micropositioner holds the TEM grid in place and allows for aligning the grid over the microchannel. Once the x-y and rotational alignment are complete, the grid is lowered down onto the microchannel. Using this setup, the alignment of the membrane can be viewed under the transmission microscope while manipulating the grid position in three dimensional space.

Using alignment marks would have led to an alignment tolerance that was on the order of the microchannel width, which in many cases was on the order of 5-10 μm. In order to improve the alignment tolerance, a square array of nanopores was created. The pitch of the nanopore array was equal to the microchannel width. This ensures that at most, a line of nanopores is deposited over the microchannel. The encapsulating PDMS piece, when placed perpendicular to the original channel then isolates a single nanopore between the two microchannels. This method increases the alignment tolerance to the width of the array, which was 80 μm for these experiments. The Focused Ion Beam (FIB) can be programmed using a NanoPattern Generation System (NPGS) to create such an array of nanopores within minutes.

Unlike a transmission electron microscope, there are focused ion beams which accept wafer size samples for milling and patterning. Furthermore, a contact mask aligner, could then be used to align the wafer with nanopores and the substrate. In good

contact aligners, alignment precision is possible down to 1-2 μm with additional tilt and rotation degrees of freedom for alignment, thereby making this amenable to wafer scale fabrication.

5.2 High Yield Transfer of Membrane

In the previous section, the setup for aligning nanopores over the microchannel was presented. The high yield transfer of the membrane from the 3mm grid to the substrate is the next pre-requisite for the successful demonstration of this technology. Patel. et. al. developed a method for transferring silicon membranes, whereby tethers to the free standing membrane were lithographically patterned over an entire wafer. Van der Waals forces allow for intimate contact and an adhesive force between the membrane and the substrate. Upon removal of the wafer, stresses are concentrated locally near the tethers, causing stress induced fracture at the tethers and allowing for the membrane to remain on the substrate [30]. This technique was developed for stacking multiple membranes on top of a mesa to create three dimensional photonic crystals.

When the membrane is transferred to a rigid substrate, particulate contamination becomes an issue and can prevent successful transfer. The use of polymeric substrates with some degree of elasticity would to some extent mitigate this problem and ensure higher transfer yield. Contact with the membrane close to the particle causes some deformation of the polymeric substrate. The energetic penalty associated with this deformation is offset by the decrease in surface energy associated with the contact. In general, in the presence of a particulate, the membrane and a PDMS substrate could be seen to contact within two particle radii.

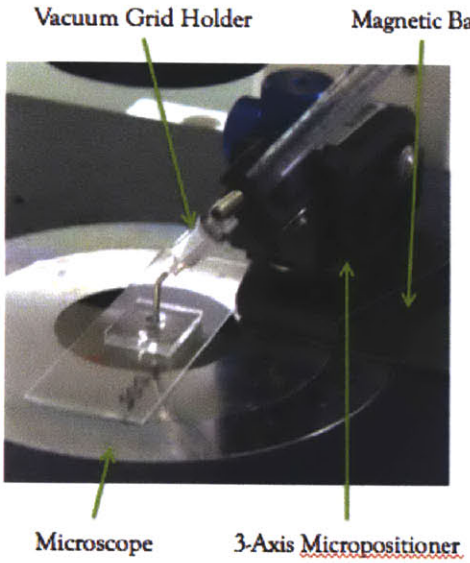

(a) Image of custom micropositioner setup

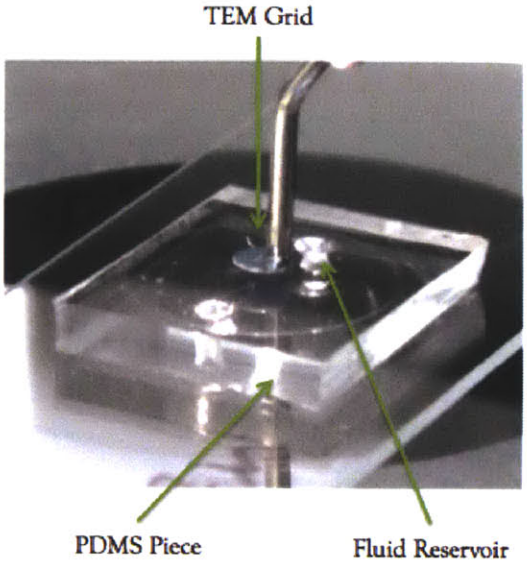

(b) Closeup of membrane during alignment over PDMS microchannel

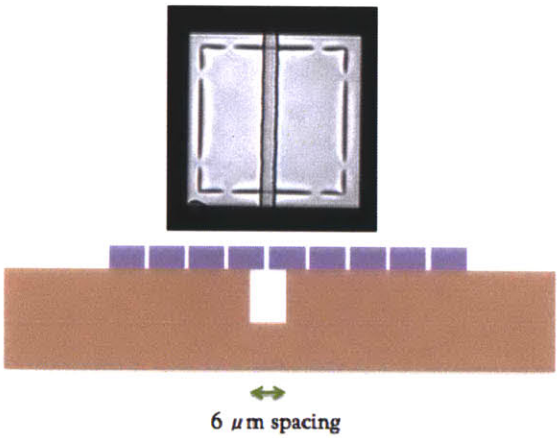

(c) Microscope image of membrane prior to removal of the TEM grid from PDMS

Figure 5.1: Positioning and Alignment of Nanopore Membrane over Microchannel

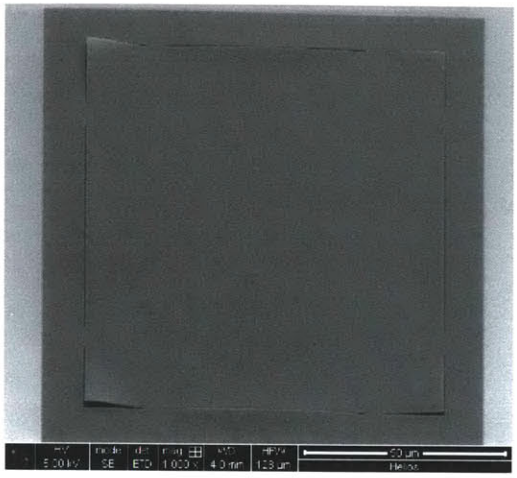

Figure 5.2: Slits made inSiN_x membrane using focused ion beam milling

As a variant to the method by Patel. et. al., slits were patterned into the membrane using a focused ion beam. The geometry of the slits can be seen in Figure 5.2. Due to the weak van der Waals bonding using this method, it was expected that infiltration of water between the membrane and the PDMS could occur, effectively de-bonding the PDMS and the membrane. In order to test for sufficient bond stability, the PDMS substrate with membrane and another identical PDMS substrate were treated with air plasma for 30 seconds at 700 mTorr of atmospheric pressure. The PDMS microchannel without the membrane was then placed on top of the first such that the microchannel patterned in it crossed perpendicular to the microchannel in the substrate with the membrane. The alignment was done within two minutes under an inverted microscope. Following this procedure, a $0.04\,mg/mL$ solution of tetramethylrhodamine-dextran (TMRD) was injected into the PDMS piece on which the membrane was deposited. The dextran conjugation of the rhodamine adds sufficient size to the molecule to prevent it from diffusing into the PDMS matrix. The device was then placed under an epifluorescence microscope and viewed with a bandpass filter whose range was 535 nm to 550 nm. Images were taken every thirty minutes for three hours, allowing the fluorescent dye to diffuse wherever the water permeates.

The results, depicted in figure 5.3, demonstrate the necessity of strong adhesive forces between the membrane with the PDMS substrate. Since SiN_x has a large proportion of native hydroxyl groups terminating its surface, plasma bonding of SiN_x to PDMS was attempted. Both a single PDMS piece and a $3mm$ grid were exposed to oxygen plasma for 15 seconds at 700 mTorr of atmospheric pressure. After four minutes, the grid was placed in contact with the PDMS, and subsequently removed after waiting another five minutes. Using this method, the bond strength was sufficiently strong to cleave the membranes off the grid without making the cuts, as shown in fig. 5.4. While this method ensured a tight irreversible bond for those membranes which transferred, the transfer yield was not as high as when the slits are made.

In order to ensure both high yield and strong bonding, final devices were made using the plasma bonding technique and the FIB patterned slits in the membrane.

5.3 Choice of PDMS Substrate

Up until the discussion of bonding SiN_x to a PDMS substrate, the device concept and preparation procedure was sufficiently general to allow for the use of any substrate, polymeric or solid state. In the actual implementation, there are significant benefits to using PDMS substrates. Data presented in the previous section demonstrated the necessity of strong bonding between the membrane and microchannel carrying substrate. PDMS can be bonded using oxygen plasma to either SiN_x or SiO_2. PDMS can also be covalently bonded to nearly any inorganic oxide material by using Deep UV exposure (254 nm) instead of oxygen plasma treatment, with bond strengths which

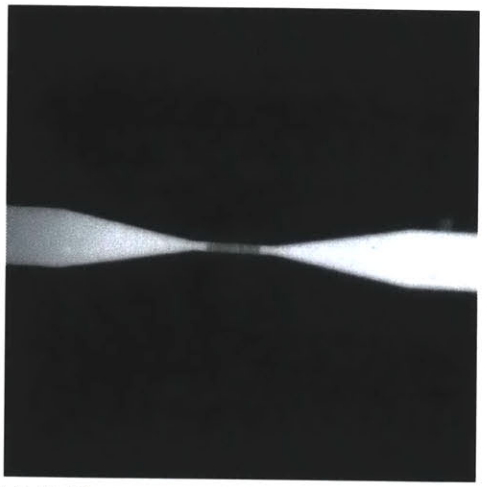

(a) Epifluorescence image after injection of fluorescent dye TMRD

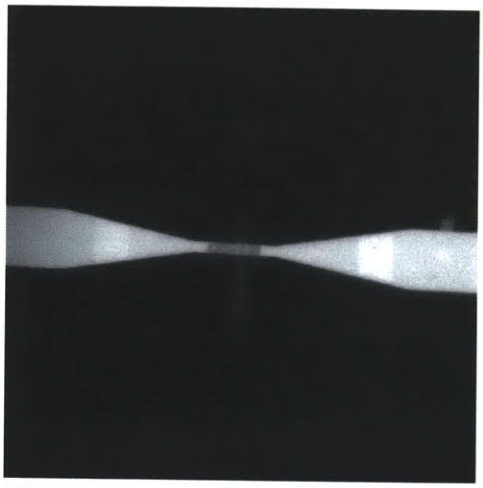

(b) Epifluorescence image after one hour

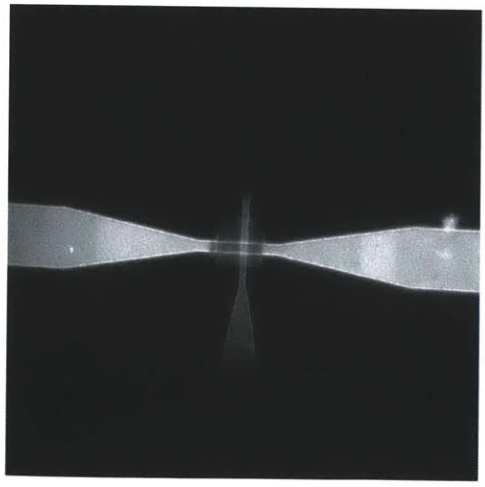

(c) Epifluorescence image after three hours

Figure 5.3: Effect of poor bonding between substrate/membrane on water infiltration

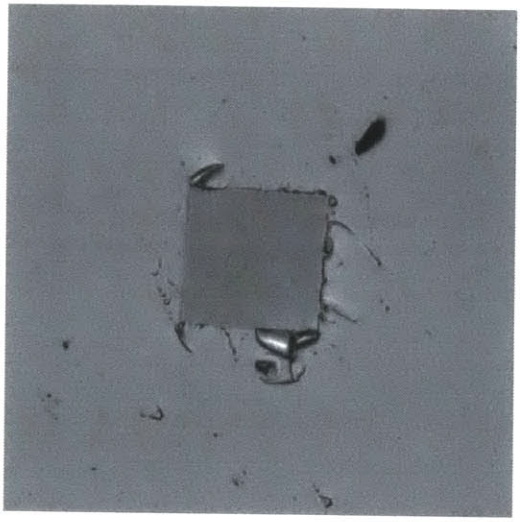

Figure 5.4: Transfer of SiN_x membrane through plasma bonding to PDMS

allow for the transfer of inorganic oxide membranes to PDMS [31, 32]. Therefore, using PDMS allows for use of a wide range of solid state materials. As an initial demonstration of the versatility of the PDMS platform, two different nanopore devices were made. The first nanopore device was fabricated with an aluminum oxide surface, and the second nanopore device with a glass surface. Since the reduction of capacitive noise is expected to arise predominantly from the removal of the silicon wafer, the variation of nanopore surface properties also acts as a negative control demonstrating that the nanopore surface is not a significant factor in the decrease in noise.

Furthermore, PDMS is one of the most widely used materials for rapid prototyping of microfluidic devices using soft-lithographic techniques, allowing proof of concept to be demonstrated much faster than with another substrate material. It will also in the future allow for seamless integration with PDMS microfluidics. Being a polymeric substrate furthermore improves the degree of conformation of the second PDMS substrate (the one without membrane) to the discontinuous topology presented by the membrane on the first substrate. Perhaps most importantly for the success of the device concept, the dissipation factor of PDMS is roughly 0.002, very similar to that of quartz/glass.

Therefore, it is expected that the PDMS will not contribute significant capacitive noise.

5.3.1 Fabrication of Aluminum Oxide Nanopore Device

A 6 μm array of 50 nm nanopores was milled into the central window of the commercially available 9 window TEM grids with 50 nm of LPCVD SiN_x grown on silicon. Slits were milled into the membrane after nanopore fabrication. PDMS was mixed in a 3:1 ratio of polymer to curing agent and poured over a SU-8 mold containing the negative image of the microchannels cured. The PDMS was cured for 4 hours at 80 degrees Celsius and then peeled off the mold. The membrane with nanopores was then aligned and bonded over the microchannel in PDMS using the method described in the previous chapter. This piece of PDMS, and an identical piece of PDMS without a membrane were then exposed to oxygen plasma for 60 seconds (700 mTorr pressure of atmospheric composition air) and bonded to each other. The composite device was placed in an oven at 80 degrees Celsius, and left for one day for full curing of the PDMS-PDMS bond. 100 cycles of atomic layer deposition (Cambridge Nanotech, Savannah) of Al_2O_3 (at a temperature of 135 degrees Celsius) was performed with an expected growth rate of 0.11 nm / cycle. The wait time between pulses was extended to 5 seconds to ensure transport of the ALD precursors throughout the chamber. This conformally coated all device surfaces, including the reservoirs, the microchannels, the membrane, and the nanopore, thereby decreasing the nanopore diameter to roughly 28 nm.

5.3.2 Fabrication of Silicon Dioxide Nanopore Device

The silicon dioxide nanopore device was made following the same protocol as the aluminum oxide device with one primary difference. The ALD of SiO_2 was performed directly after nanopore fabrication (and before making the slits in the membrane) instead of after the complete assembly of the device. ALD of SiO_2 was performed at 250

degrees Celsius, and contained a small fraction of alumina in it to facilitate the growth process.

Chapter 6

Device Characterization and Testing

Having fabricated devices satisfying the principal requirements outlined above, the goal of device testing was to demonstrate:

1. Resistance through current pathways parallel to the nanopore is large compared to the nanopore resistance
2. Equilibrium noise levels contain negligible contributions from capacitive noise
3. DNA translocation can be detected in the fabricated devices

6.1 Leakage Current

In order for the nanopore sensor to function correctly, all current pathways in parallel to the nanopore should have a significantly larger resistance than the nanopore resistance. This criterion ensures that the parallel current pathways do not reduce the relative translocation amplitude. To test the resistance of the parallel pathways, a device was fabricated with the same procedure as the SiO_2 nanopore, with the exception that the nanopores were not fabricated in the membrane. In the absence of the nanopore, the lowest resistance between the two microchannels could be measured. The device was

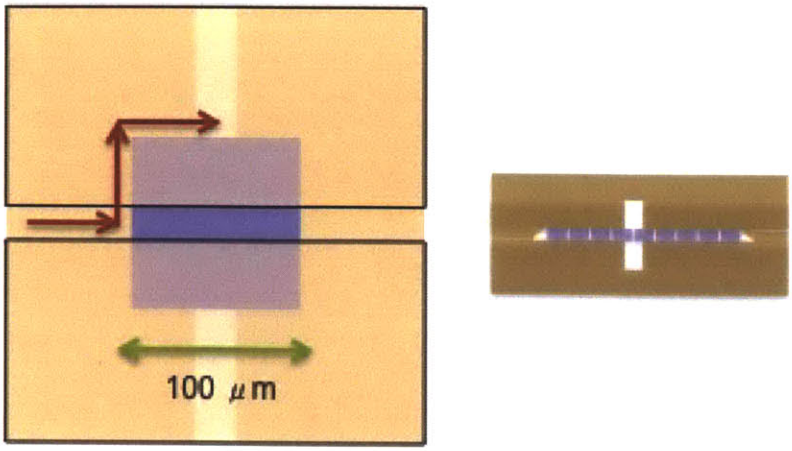

Figure 6.1: Schematic of leakage current pathway

filled with 1 M KCl, and the resistance between the two microchannels was obtained by performing an IV curve measurement with voltages varying from $\pm 1V$. In order to measure the IV Curves, the maximum voltage was set as either 1 V, or the voltage where the current was 10 nA. The voltage was then ramped down from the maximum voltage to its corresponding negative value in 21 steps using an automated Labview routine. Measurements were recorded at a 2 kHz bandwidth and a sampling rate of 10 kHz. Each voltage step was maintained for 1 second so that sufficient time was allowed for capacitive transients to decay over the interval.The resistance of the parallel current pathways was measured as 700 MΩ.

We hypothesized that the leakage current was being contributed from the inability of the second PDMS piece to conform perfectly to the sharp jump in height due to the finite membrane width, (see Figure 6.1). The length of the channel resulting from this conduit would be 100 μm, and its cross sectional area was estimated as a triangle with height and base lengths equal to the membrane thickness. First principles estimation of the resistance of this channel (using the standard equation $R = \frac{\rho L}{A}$), suggested

a resistance of 750 MΩ, which is very similar to the experimentally measured value. To further validate the results, fluorescence tests were performed using the procedure outlined in the previous chapter. The appearance of a fluorescent outline around the membrane further supports the conclusion that the channel is around the sides of the membrane due to the step height.

Importantly, the leakage resistance is significantly higher than the typical nanopore resistance which is on the order of 30 - 50 MΩ.

6.2 Noise Characterization

The hypothesis on which this whole work was based on was that the removal of the silicon wafer backing would virtually eliminate capacitive noise. In order to test the hypothesis, a method for measuring the capacitive noise of the fabricated devices was required. The unified noise model presented in Chapter 2 predicted the existence and magnitude of several sources of noise:

1. Measurement Noise
2. Resistive Noise
3. Capacitive Noise
4. Non-Equilibrium Noise

Since non-equilibrium noise only exists in the presence of a driving force, by measuring the RMS noise in the absence of an applied voltage, non-equilibrium contributions to the noise could be neglected. Both measurement and resistive noise, however, are fundamental sources of noise and could not be removed. This means that capactive noise contribution to the total noise would have to be differentiated from the contributions from measurement and resistive noise. However, it was imperative that the noise model

itself was first verified. In particular, the measurement noise expression had in it a fitting parameter. The measurement instrument used in these experiments was Axopatch 200B (Molecular Devices, Inc.). The amplifier was set to $\beta = 1$ (amplifier specific setting), and an additional output gain of $\alpha = 1$. By comparing the RMS noise measured by the in-built 5 kHz analog filter to the noise measured after digitization, we verified that digitizer noise was negligible in these experiments.

Thus, in order to calibrate the measurement noise and resistive noise, the noise arising from high quality resistors was first measured. The resistors had resistances in the range of 10 MΩ to 5 GΩ, and had very low capacitance C $<$ 1 pF and negligible inductance. Therefore, we reasoned that in the absence of an applied voltage, noise measurements through the resistor would correspond to measurement noise and resistive noise only. Assuming that resistive noise followed the theoretical prediction of $\delta I_R = 4k_BT/R$, the measurement noise model could be calibrated. Following the calibration of the measurement noise, the noise as a function of resistance for a system with only resistive and measurement noise could be predicted.

Next, noise and resistance in both the aluminum oxide and silicon dioxide nanopores were measured as a function of concentration. For each measured concentration, the resistance was calculated from IV curve data, (Figure 6.2). Figures 6.3 and 6.4 show the resistance as a function of concentration for the two different nanopore devices. Figure 6.4 also contains data for a nanopore device on which no atomic layer deposition was performed, thereby illustrating both the increased resistance due to pore shrinking and the effects of surface charge on the resistance.

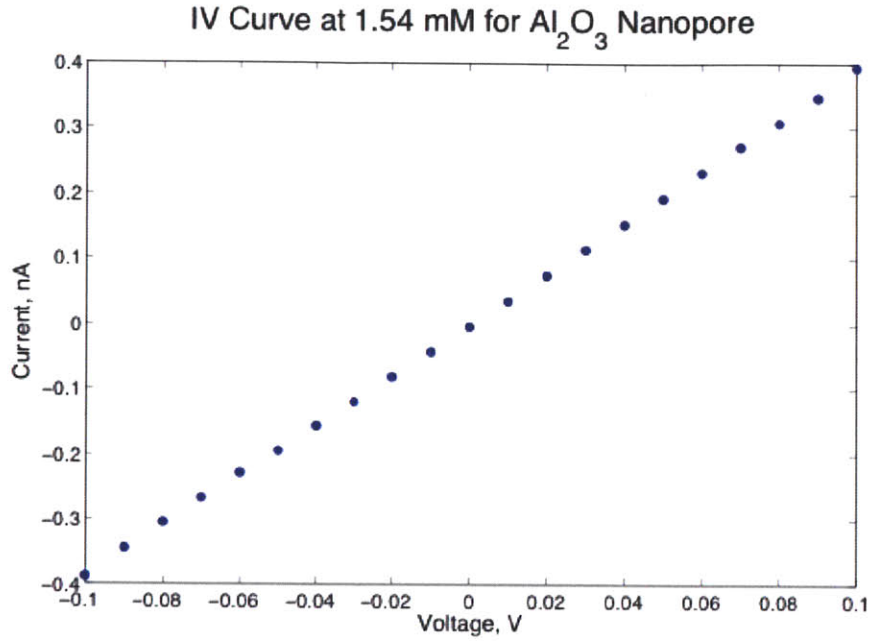

Figure 6.2: IV Curve for Al_2O_3 nanopore at 1.54 mM KCl

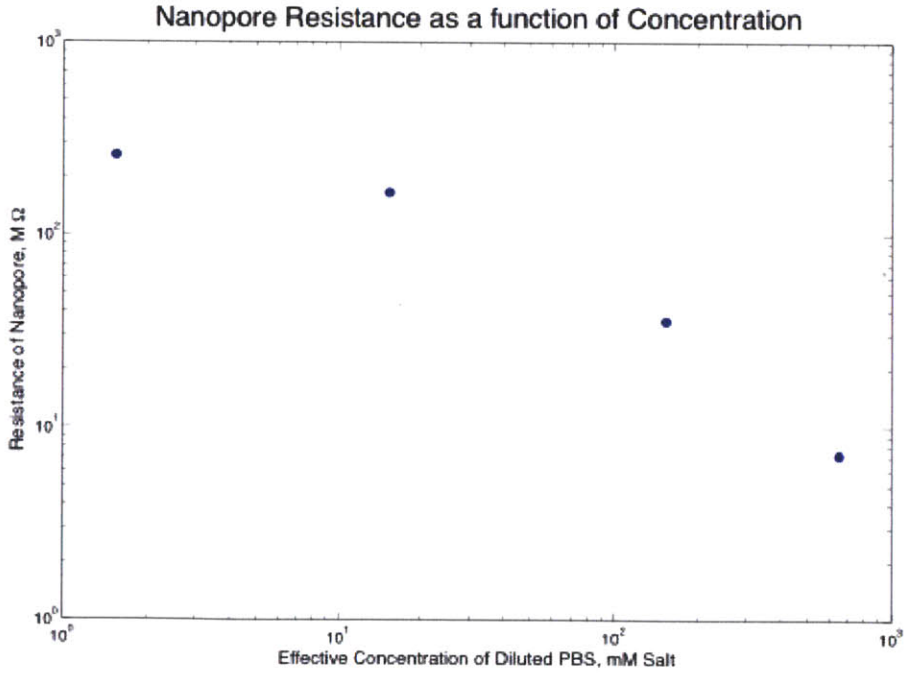

Figure 6.3: Concentration versus resistance for the Al_2O_3 device

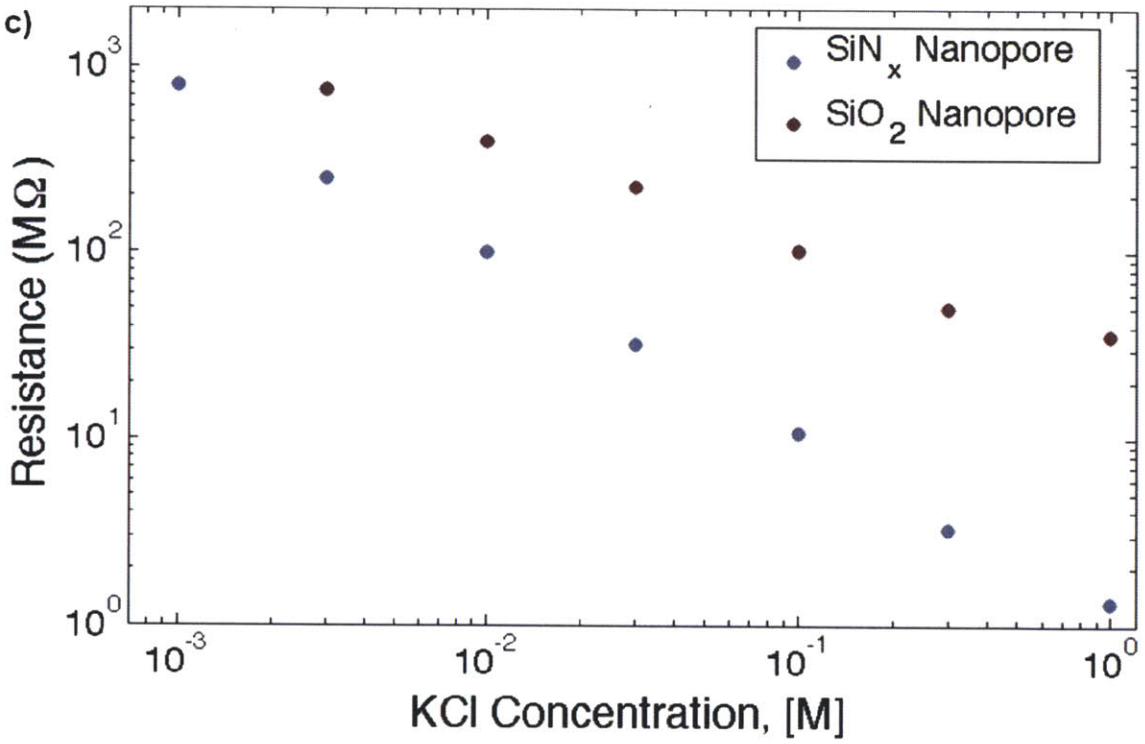

Figure 6.4: Concentration versus resistance for a SiO_2 coated device and a device without the ALD coating

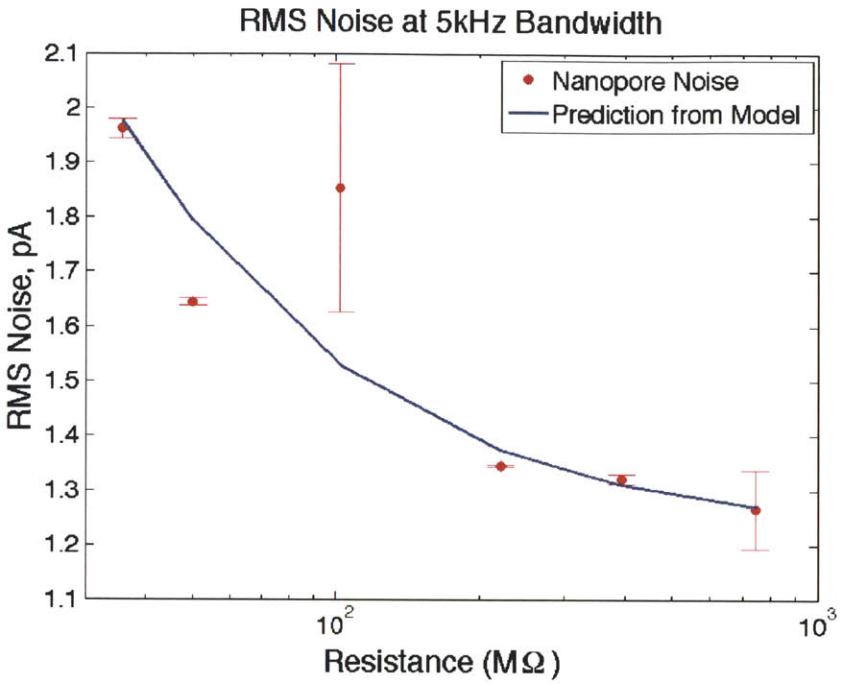

Figure 6.5: Noise measurements at 5 kHz (silicon dioxide nanopore).

Having obtained the resistance, the noise at each of those concentrations was also measured. Noise measurements were performed at 5 kHz and 100 kHz Bessel filter bandwidths in the absence of an applied voltage. The sampling bandwidth, as per Nyquist's theorem, was set to twice the filtering frequency in order to prevent aliasing of frequencies. Three current traces were recorded, each two seconds in duration, for each concentration. From them, the noise was calculated by subtracting off any baseline drift, and then computing the RMS fluctuations about the mean current. The RMS current fluctuations (RMS noise) was then compared to the predicted noise from a system with only resistive and measurement noise (Figures 6.5 and 6.6).

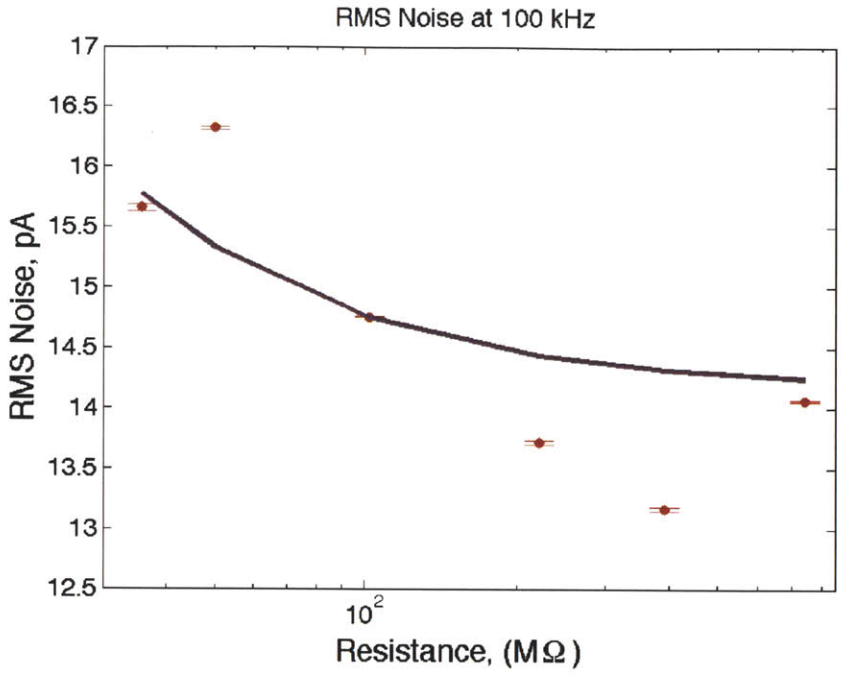

Figure 6.6: Noise measurements at 100 kHz (silicon dioxide nanopore).

The close agreement between the resistive/measurement noise prediction and the experimental data demonstrate that capacitive noise is relatively unimportant in the system. The absence of capactive noise was verified by the flat power spectral density at high frequencies. Noise measurements from the aluminum oxide nanopore yielded nearly identical results. Figure 6.7 plots the noise levels in comparison with the noise levels of a typical nanopore device in which capacitive noise from the silicon wafer is still present. The results clearly indicate that removing the silicon wafer backing has reduced the RMS noise by a factor of two.

6.3 DNA Translocation Data

Next, λ-phage DNA (48.5 kbp, purchased from New England Biolabs) was mixed with 1 M KCl electrolyte solution and injected into one side of the device. All DNA transloca-

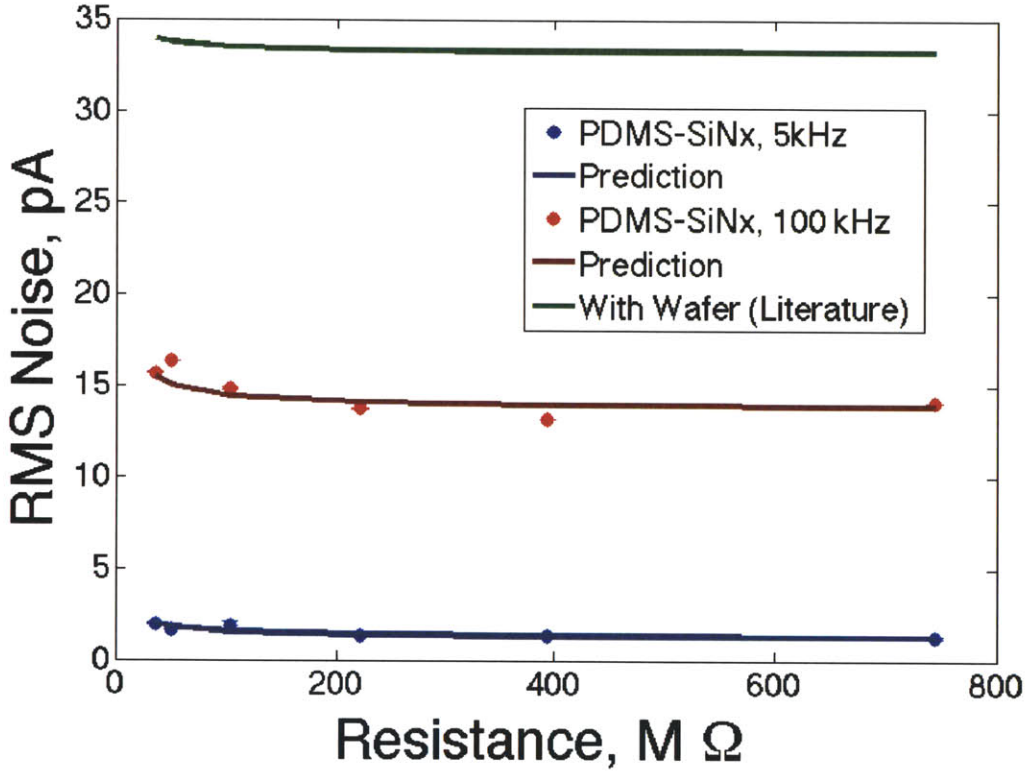

Figure 6.7: Plotting prior data in direct comparison to equivalent circuit model predictions from literature

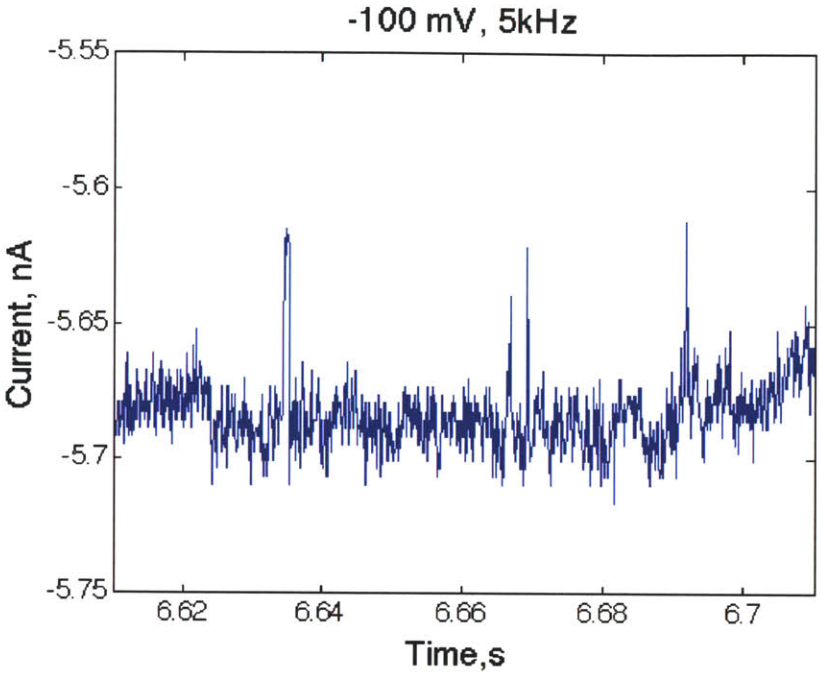

Figure 6.8: λ - DNA translocation events with 5 kHz analog filter at -100 mV (Al_2O_3 nanopore)

tion data presented here was measured through the aluminum oxide nanopores. While similar translocation data was observed in the silicon dioxide nanopore, it is not presented in order to keep the surface characteristics constant as the measurement conditions are changed. The initial concentration of DNA was 1 μg/mL. Ag/AgCl electrodes were placed on opposite sides of the membrane, and a 100 mV voltage bias was applied. The analog 8 pole Bessel filter was set to 5 kHz and a sampling bandwidth of 10 kHz. The resultant DNA translocation rate was roughly 6 translocations per second, with typical translocation duration between 500 μs and 2 ms (Figure 6.8). The mean amplitude at this bandwidth was $\Delta I = 65 \pm 10\,pA$. In some cases, the translocation duration was significantly larger, indicating transient DNA adhesion to the nanopore walls (Figure 6.9).

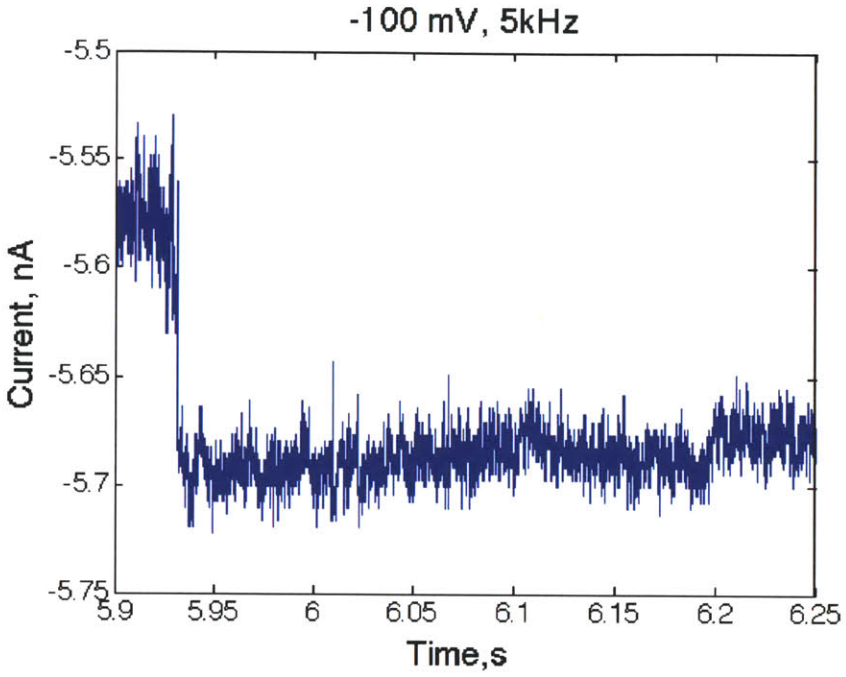

Figure 6.9: Transient DNA adhesion to the nanopore (Al_2O_3 nanopore)

Since the translocation duration was close to the corresponding cutoff frequency of the 5 kHz filter, we reasoned that the signal might have different amplitude characteristics at a higher analog filter frequency provided DNA could be detected above the baseline noise levels. Furthermore, since many translocations consisted of only a few samples, it was possible that some translocations were ignored due to the inability to distinguish the current spike from random fluctuations. Thus, measurements were taken next at a 100 kHz analog Bessel filter with a sampling bandwidth of 200 kHz, keeping the same applied voltage. In this case, slightly over 60 translocations were detected in the first second of measurement alone. While many of the translocations still had a similar duration between 500 μs to 2 ms, by this time, it seemed as if a larger percentage of translocation events were demonstrating enhanced DNA -pore interactions. Nonetheless, the translocation amplitude for all events, irrespective of the DNA

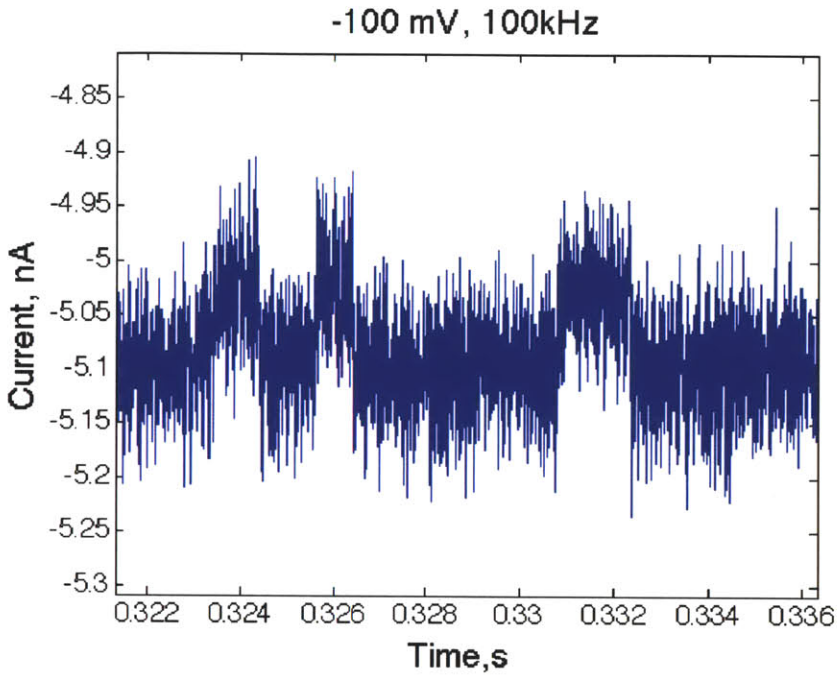

Figure 6.10: λ - DNA translocation events with 100 kHz analog filter at -100 mV (Al_2O_3 nanopore)

- pore interactions was slightly larger at $\Delta I = 98 \pm 10\,pA$. This result suggests that higher bandwidths improve the resolution of the translocation amplitude, in particular due to filter attenuation. The effects of the analog filter on translocation amplitude and duration has been studied in greater detail by Pedone et. al.[33].

The 500 μs translocation time corresponds to roughly 10 ns/bp. Assuming that the translocation amplitude remains unchanged down to a translocation duration of 2 μs, it should be possible to detect and measure the amplitude of 2 kbp DNA without any filter artifacts. For smaller DNA molecules, the translocation amplitude is expected to be attenuated, and consequently, the signal size for this nanopore cross sectional area becomes too small for detection. Therefore, for detecting smaller molecules, a smaller nanopore should be used. At the moment, nearly all detection of DNA molecules

smaller than 500 bp in nanopore devices is done in the regime where the translocation amplitude is non-trivially attenuated due to the short translocation duration compared to the corresponding filter cutoff. To prevent this, the DNA translocation must be slowed down (and preferably, not from DNA-pore interactions).

Chapter 7

Conclusion

In this thesis, a novel device design for addressing the central problem of low signal to noise ratio in nanopore devices was developed. The device concept involves the transfer of solid state membranes into microfluidic devices.

Signal and noise theory was investigated to thoroughly understand the benefits of this approach. Analytical expressions for the mean change in current during analyte translocation was derived, and examples of the mathematical inference between molecular cross sectional area and mean current were presented. By virtue of the nature of the inference, precision in current measurements is directly related to precision in the inference in molecular structure. The measurement precision, however, is limited by current fluctuations, which restrict the ability to discriminate between changes in the mean current. By constructing a thorough noise model, capacitive noise from the silicon wafer handle was demonstrated to be the dominant source of noise.

The recapture theory in one dimension, and full 3D simulations of the electric field demonstrate that the use of microchannels to confine the electric field can enhances the potential to perform multiple measurements on analyte molecules in nanopore sensors. In the device design, the microchannels have the additional effect of defining the exposed

membrane area, thereby limiting the capacitance (and capacitive noise) of the system. Therefore, that the proposed membrane transfer process addresses the key challenge of inference uncertainty by virtually eliminating capacitive noise, confining the electric field outside the nanopore, and retaining compatibility with pre-existing fabrication techniques for solid state nanopores.

Realization of the device concept required a method for alignment of the nanopore over the microchannel, and a method for high yield transfer of the membrane to the substrate. The alignment procedure was carried out by creating a square array of nanopores with the array pitch equal to the microchannel width. This ensured that one nanopore would be encapsulated between the two perpendicular microchannels. In order to transfer the membrane with high yield, a combination of plasma bonding and FIB patterned slits in the membrane were used. PDMS was chosen as the microchannel substrate material, as it affords flexibility in substrate material choices, and ease of integration with microfluidics.

Following device fabrication, the devices were tested to ensure sufficient integrity for performing noise measurements and DNA translocation experiments. Noise levels were found to be a factor of two lower than the state-of-the art nanopore devices, with a virtual elimination of capacitive noise. This is a significant result that allows for increasing the measurement bandwidth. DNA detection experiments were performed with λ-DNA. By performing DNA detection at both $5kHz$ and $100kHz$, the significance of using appropriately high analog filter bandwidths was highlighted.

Thus, this work has demonstrated the hypothesized reduction in capacitive noise, thereby making the use of higher bandwidths ($\geq 100kHz$) feasible for nanopore experiments. At these larger bandwidths, noise is now limited by the measurement apparatus, and further improvements must be obtained by appropriate amplifier design.

Bibliography

[1] J.J Kasianowicz, E Brandin, D Branton, and D.W Deamer. Characterization of individual polynucleotide molecules using a membrane channel. *Proceedings of the National Academy of Sciences of the United States of America*, 93(24):13770, 1996.

[2] J Clarke, H.C Wu, L Jayasinghe, A Patel, S Reid, and H Bayley. Continuous base identification for single-molecule nanopore dna sequencing. *Nature Nanotechnology*, 4(4):265–270, 2009.

[3] Ian M Derrington, Tom Z Butler, Marcus D Collins, Elizabeth Manrao, Mikhail Pavlenok, Michael Niederweis, and Jens H Gundlach. Nanopore dna sequencing with mspa. *PNAS*, pages 1–6, Aug 2010.

[4] C Dekker. Solid-state nanopores. *Nature Nanotechnology*, 2(4):209–215, 2007.

[5] M Wanunu, T Dadosh, V Ray, J Jin, L McReynolds, and M Drndić. Rapid electronic detection of probe-specific microrna using thin nanopore sensors. *Nature Nanotechnology*, 5(11):807–814, 2010.

[6] S Garaj, W Hubbard, A Reina, J Kong, D Branton, and JA Golovchenko. Graphene as a subnanometre trans-electrode membrane. *Nature*, 467(7312):190–193, 2010.

[7] C.A Merchant, K Healy, M Wanunu, V Ray, N Peterman, J Bartel, M.D Fischbein, K Venta, Z Luo, and A.T.C Johnson. Dna translocation through graphene nanopores. *Nano Letters*, pages 580–1132, 2010.

[8] G.F Schneider, S.W Kowalczyk, V.E Calado, G Pandraud, H.W Zandbergen, L.M.K Vandersypen, and C Dekker. Dna translocation through graphene nanopores. *Nano Letters*, pages 1146–1153, 2010.

[9] V Dimitrov, U Mirsaidov, D Wang, T Sorsch, W Mansfield, J Miner, F Klemens, R Cirelli, S Yemenicioglu, and G Timp. Nanopores in solid-state membranes engineered for single molecule detection. *Nanotechnology*, 21:065502, 2010.

[10] RMM Smeets, UF Keyser, NH Dekker, and C Dekker. Noise in solid-state nanopores. *Proceedings of the National Academy of Sciences*, 105(2):417, 2008.

[11] V Tabard-Cossa, D Trivedi, M Wiggin, NN Jetha, and A Marziali. Noise analysis and reduction in solid-state nanopores. *Nanotechnology*, 18:305505, 2007.

[12] M Gershow and JA Golovchenko. Recapturing and trapping single molecules with a solid-state nanopore. *Nature Nanotech*, 2(12):775–779, 2007.

[13] R Fan, R Karnik, M Yue, D Li, A Majumdar, and P Yang. Dna translocation in inorganic nanotubes. *Nano Letters*, 5(9):1633–1637, 2005.

[14] M Wanunu, J Sutin, B McNally, A Chow, and A Meller. Dna translocation governed by interactions with solid-state nanopores. *Biophysical Journal*, 95(10):4716–4725, 2008.

[15] U Mirsaidov, J Comer, V Dimitrov, A Aksimentiev, and G Timp. Slowing the translocation of double-stranded dna using a nanopore smaller than the double helix. *Nanotechnology*, 21:395501, 2010.

[16] D Fologea, E Brandin, J Uplinger, D Branton, and J Li. Dna conformation and base number simultaneously determined in a nanopore. *Electrophoresis*, 28(18):3186–3192, 2007.

[17] van der Ziel. *Noise in Solid State Devices and Circuits.* John Wiley and Sons, 1986.

[18] RMM Smeets, NH Dekker, and C Dekker. Low-frequency noise in solid-state nanopores. *Nanotechnology*, 20:095501, 2009.

[19] J.D Uram, K Ke, and M Mayer. Noise and bandwidth of current recordings from submicrometer pores and nanopores. *ACS nano*, 2(5):857–872, 2008.

[20] LI Berge, J Feder, and T Jøssang. A novel method to study single particle dynamics by the resistive pulse technique. *Review of scientific instruments*, 60(8):2756–2763, 1989.

[21] C.H Reccius, J.T Mannion, J.D Cross, and HG Craighead. Compression and free expansion of single dna molecules in nanochannels. *Phys. Rev. Lett.*, 95(26):268101, 2005.

[22] A.E Nkodo, J.M Garnier, B Tinland, H Ren, C Desruisseaux, L.C McCormick, G Drouin, and G.W Slater. Diffusion coefficient of dna molecules during free solution electrophoresis. *Electrophoresis*, 22(12):2424–2432, 2001.

[23] A. J Storm, J. H Chen, X. S Ling, H. W Zandbergen, and C Dekker. Fabrication of solid-state nanopores with single-nanometre precision. *Nat Mater*, 2(8):537–540, Aug 2003.

[24] J Li, D Stein, C McMullan, D Branton, M.J Aziz, and J.A Golovchenko. Ion-beam sculpting at nanometre length scales. *Nature*, 412(6843):166–169, 2001.

[25] M van den Hout, A.R Hall, M.Y Wu, H.W Zandbergen, C Dekker, and N.H Dekker. Controlling nanopore size, shape and stability. *Nanotechnology*, 21:115304, 2010.

[26] P Spinney, D Howitt, R Smith, and S Collins. Nanopore formation by low-energy focused electron beam machining. *Nanotechnology*, Jan 2010.

[27] L.D Menard and J.M Ramsey. Fabrication of sub-5 nm nanochannels in insulating substrates using focused ion beam milling. *Nano Letters*, page 595, 2011.

[28] P Chen, T Mitsui, DB Farmer, J Golovchenko, RG Gordon, and D Branton. Atomic layer deposition to fine-tune the surface properties and diameters of fabricated nanopores. *Nano Letters*, 4(7):1333–1337, 2004.

[29] B Schiedt, L Auvray, L Bacri, G Oukhaled, A Madouri, E Bourhis, G Patriarche, J Pelta, R Jede, and J Gierak. Direct fib fabrication and integration of. *Microelectronic Engineering*, 87(5-8):1300–1303, 2010.

[30] A.A Patel and H.I Smith. Membrane stacking: A new approach for three-dimensional nanostructure fabrication. *Journal of Vacuum Science & Technology B: Microelectronics and Nanometer Structures*, 25:2662, 2007.

[31] WM Choi, J Song, DY Khang, H Jiang, YY Huang, and JA Rogers. Biaxially stretchable "wavy" silicon nanomembranes. *Nano Lett*, 7(6):1655–1663, 2007.

[32] Y Sun, WM Choi, H Jiang, YY Huang, and JA Rogers. Controlled buckling of semiconductor nanoribbons for stretchable electronics. *Nature Nanotech*, 1(3):201–207, 2006.

[33] D Pedone, M Firnkes, and U Rant. Data analysis of translocation events in nanopore experiments. *Analytical chemistry*, 81(23):9689–9694, 2009.